Construction of an array of photonic crystal films for visual differentiation of water/ethanol mixtures

by

Mohammad Heshmat

B.Sc., University of Tehran, 2016

Thesis Submitted in Partial Fulfillment of the
Requirements for the Degree of
Master of Science

in the
Department of Chemistry
Faculty of Science

SIMON FRASER UNIVERSITY
Spring 2019

Approval

Name:	**Mohammad Heshmat**
Degree:	**Master of Science**
Title:	**Construction of an array of photonic crystal films for visual differentiation of water/ethanol mixtures**
Examining Committee:	**Chair:** Michael Eikerling Professor
	Paul C. H. Li Senior Supervisor Professor
	Vance E. Williams Supervisor Associate Professor
	Luis Sojo Supervisor Adjunct Professor
	Hua-Zhong (Hogan) Yu Internal Examiner Professor
Date Defended/Approved:	March 14, 2019

Abstract

A photonic crystals films (PCF) which consists of a porous layered structure with a highly ordered periodic arrangement of nanopores has been used to differentiate between various mixtures of water and ethanol (EtOH). Refractive index difference between the wall (silica) and air which occupies the empty pore results in the structural color of the PCF. This color disappears when the nanopores are infiltrated by a liquid with a similar refractive index to silica (or silicon dioxide). The disappearance of the structural color provides a means to construct a sensor to differentiate various water/EtOH mixtures based on their wettability of the nanopores in the PCF.

In this study, an array of silica-based PCFs was synthesized on a silicon substrate with a precise control of nanopore properties using the co-assembly/sedimentation method. Using this method, we benefitted from having different PCFs on a single substrate. Chemical coatings, neck angles, and thicknesses on each PCF were the three factors used to adjust the wettability of the pores. Nanopore wetting by water/EtOH mixtures was studied in a systematic manner and combinations of the three factors were used to develop a sensor for differentiation of various water/EtOH mixtures. The final developed sensor consisting of an array of six PCFs was able to differentiate seven different water/EtOH mixtures: W10, W20, W30, W40, W50, W60 and W70, in which W10 means 10% of water in EtOH.

Keywords: Photonic crystal film; structural color; nanopores; water/ethanol mixture; sensor

Acknowledgements

I would like to thank Dr. Paul Li for giving me the great opportunity to work with him as a graduate student. This project would not have been possible without his continuous support and invaluable guidance. I deeply appreciate his support and guidance during my study.

I am thankful to my two committee members, Dr. Vance Williams and Dr. Luis Sojo for their critical reviews of my research and helpful advices during my research project.

I would like to thank Dr. Daniel Leznoff for the use of the fiber optic spectrometer, Dr. Xin Zhang for training in SEM, Christopher Oberc and my other colleagues for their support and encouragement during my research project.

Finally, I would like to thank all my friends and family for their continuous support in pursuing my academic goals.

Table of Contents

List of Tables

List of Figures

List of Acronyms

φ_0	Neck angle
V_p	Volume of particle
m_p	Mass of particle
n_{eff}	Average refractive index of the photonic crystal
γ_{LV}	Liquid-vapor surface tension
γ_{SL}	Solid-liquid surface tension
γ_{SV}	Solid-vapor surface tension
η_f	Viscosity of fluid
θ_C	Contact angle of fluid
θ_i	Angle of incidence light
ρ_f	Density of fluid
ρ_p	Density of particle
3FS	Trichloro (3,3,3-trifluoropropyl)-silane
9FS	Nonafluorohexyltrichlorosilane
EtOH	Ethanol
EXR	Excess over theoretically required amount of TEOS
F_b	Buoyancy force
FCC	Face-centred cubic
F_d	Drag force
F_g	Force of gravity
g	Acceleration of gravity
HF	Hydrofluoric acid
N	Number of pores in unit cell
PCF	Photonic crystal film

PMMA	poly (methyl methacrylate)
R	Radius of pore
TEOS	Tetraethylorthosilicate solution
TMS	Methyltrichlorosilane
TPMA	3-(Trichlorosilyl) propyl methacrylate
a	Gradient of particle velocity with respect to the time
r	Radius of particle
α	Unit cell parameter
v	Velocity of particle

Chapter 1.

Introduction

To explain what photonic crystals are and what roles they can have in our lives, we need to have a better understanding of colors and their production mechanisms. Basically, color can be produced in different ways. One mechanism of color production is based on absorption of light. The light traveling toward an object consists of different wavelengths. Some of these wavelengths are absorbed by the object while remaining are reflected or transmitted. The color of an object is determined by those wavelengths of light which are reflected or transmitted. In another mechanism, the color production is originated from diffraction or interference of light through materials consisting of a periodic structure.[1]

1.1. Photonic crystals

Photonic crystals (PC) were introduced by Yablonovitch[2] and John[3] for the first time. Yablonovitch showed that there was an electromagnetic band gap in a three-dimensional periodic structure in which certain wavelengths are forbidden to pass through. John showed that a strong localization of photons in some disordered media would occur within certain ranges of frequencies. These two ideas paved the way for the introduction of photonic crystals.[4,5]

1.1.1. Photonic crystals properties

Photonic crystals are periodic nanostructured materials which can control how photons are absorbed by or reflected from them. These materials can allow certain wavelengths to be reflected while blocking the remainder. Similar to the electronic band gap in semiconductors, each photonic crystal has a unique optical band gap. Optical band gap of a photonic crystal refers to a range of light wavelengths that cannot be reflected from the crystal. These wavelengths are called the modes and a group of modes is called the band.[4]

1.1.2. Photonic crystals types

Photonic crystals are composed of periodic structures that consist of at least two different dielectric constants. Dielectric constant (or relative permittivity) of a substance is the factor by which the electric field between the charges in it is decreased relative to vacuum.[6] According to their dielectric constant configuration, the photonic crystals can be classified in three different types: 1) One-dimensional (1D) photonic crystals that have periodic dielectric constant in one direction. These materials can be created by depositing a layer of high-refractive-index material and a layer of low-refractive-index material periodically. Bragg mirror (or dielectric mirror) is an example of 1D photonic crystals which can be used to enhance the efficiency of solar cells.[4,1] 2) Two-dimensional (2D) photonic crystals that have periodic dielectric constants in two different directions. 3) Three-dimensional (3D) photonic crystals in which dielectric constants are periodically repeated in three different directions. Fig 1.1 shows the schematic diagrams of different types of photonic crystals and their dielectric constant configurations.[7,8]

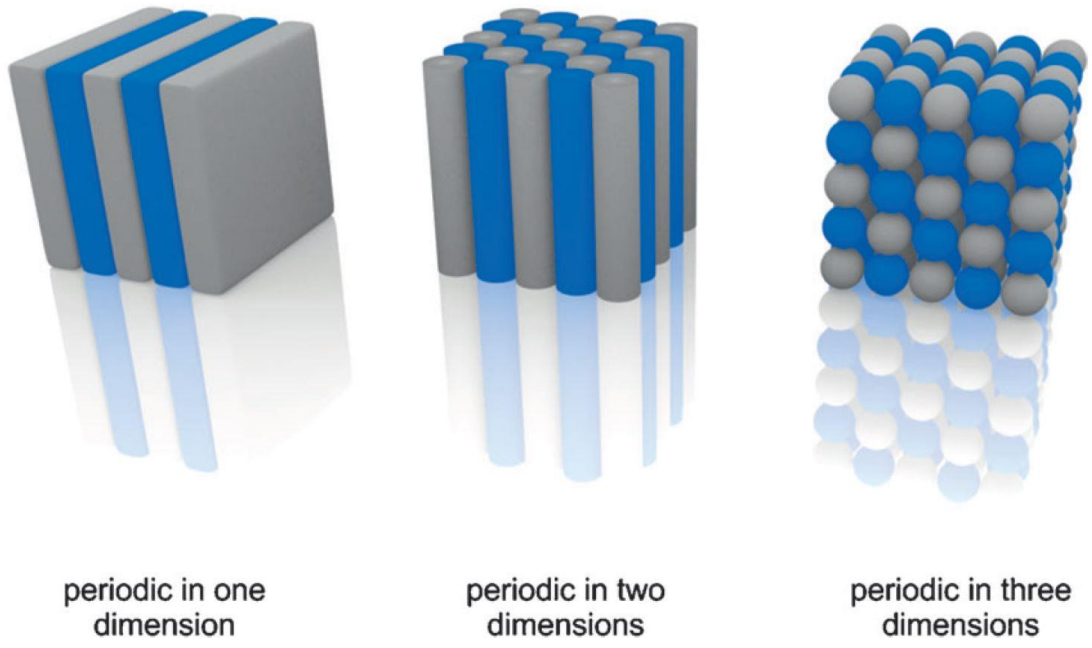

Figure 1.1. Schematic representation of dielectric constant configuration in 1D, 2D and 3D photonic crystals.
Photo is Reproduced with permission.[8]

1.1.3. Fabrication of three-dimensional photonic crystals

There are generally two approaches for the fabrication of photonic crystals: 1) top-down 2) bottom-up. Top-down methods, such as multibeam holography[9] and phase mask lithograph[10], offer high precision and resolution to the final photonic crystal structure. However, these methods are known to be complicated, tedious and expensive, since they need complex equipment. On the other hand, by using the bottom-up approach, researchers have been able to produce high quality photonic crystals in an easier, cheaper and faster way. In the bottom-up approach, the small building blocks are self-assembled to produce periodic ordered structures. For this purpose, spherical colloidal beads are most commonly used as the small building blocks.[11]

1.2. Colloidal forces and interactions

Colloidal particles have a considerably high ratio of surface area to volume and their particle diameters range from nanometers to micrometers. Therefore, it is of great importance to consider interactions between the surfaces of the colloidal particles when studying their final physical state.[12] The colloidal particles which are being used in fabrication of 3D photonic crystals are usually made of polymers such as polystyrene (PS) or poly (methyl methacrylate) (PMMA) or they are made of silica. These spherical particles will be self-assembled if the interparticle forces are sufficiently balanced.[11,13] To understand the mechanism behind this self-assembly, different forces between colloidal particles should be taken into account.

There are three different types of forces responsible for interactions between these colloidal particles. First, it is the van der Waals' attraction force which leads to an ordered packing of colloidal particles. For spherical colloids the most thermodynamically favored structure is face-centered cubic (fcc) (Fig. 1.2.) with the crystalline packing density of 74% volume filling.[14] Hexagonal close-packed (hcp) is also a favored structure in some cases.[13] Second, it is the repulsion forces that can exist to prevent any particle agglomeration to occur as a result of van der Waals' attraction forces. There are different kinds of repulsion forces like electrostatic repulsions[15] in which two species with the same charge drive away each other in a polar solvent.[11] The repulsive force of particles should be in a certain range, exceeding which may affect the close-packing process of particles. At the same time,

insufficient repulsive force will lead to particle agglomeration.[16] Third, it is the external forces such as gravity or centrifugal force that will bring particles together.[11]

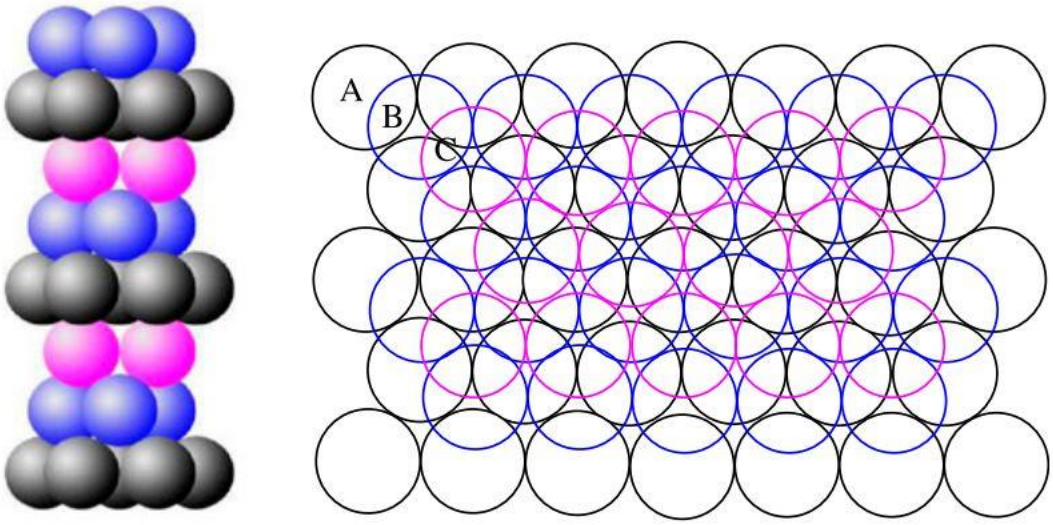

Figure 1.2. 3D (left) and top view (right) of a face-centered cubic (FCC) structure (ABC close-packing structure).
Photo is Reproduced with permission.[17]

Other than shape, size and charge, other factors such as temperature and concentration can have effects on the interparticle forces and consequently on the final colloidal structure.[12]

1.3. Inverse Opals

3D colloidal photonic crystals can be classified as opals and inverse opals. Opals consist of silica or polymeric nanospheres that can be produced by assembly of colloidal particles, followed by a drying step. On the other hand, inverse opals are fabricated when opals are used as the template to replicate their structures. The fabrication of inverse opals generally involves three steps: 1) the template material (e.g., polymer latex or silica spheres) is deposited onto a substrate. Thin colloidal crystal film (PCF) can be produced using solvent evaporation. 2) the matrix phase is then infiltrated into the preassembled colloidal template. Matrix can be a liquid, which can infiltrate the interstitial space of the template by capillary forces. Examples of the matrix can be a sol-gel precursor to a ceramic material, a precursor of a polymer, a monomer with an initiator, or it can be a gaseous precursor. 3) the template is then selectively removed which leaves behind a

nanoporous ordered structure in the matrix. Depending on the type of template, its removal can be done by calcination (or thermal decomposition) at high temperatures (e.g. above 300°), or chemically by solvent extraction (e.g. using toluene, chloroform or hydrofluoric acid), or by air/oxygen plasma treatment.[1] Fig. 1.3 schematically shows the different steps for fabrication of inverse opals. The pore diameters of the obtained inverse opals range from tens of nanometer to several microns.[18]

Several advantages have been reported for using polymeric colloidal particles as the template to fabricate inverse opals. These polymeric templates are low-cost, and their size, shape and chemical composition are tuneable. Compared to silica templates which require hydrofluoric acid to be removed, polymeric templates can be easily removed using calcination at high temperatures or solvent extraction with less hazardous materials.[19,20]

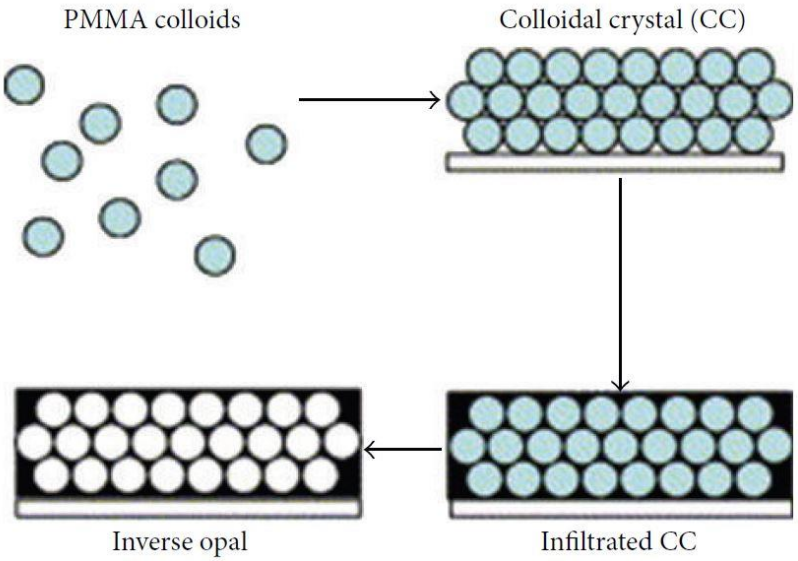

Figure 1.3. Different stages during inverse opal fabrication.
Photo is Reproduced with permission.[21]

Fig. 1.4 represents a unit cell of an infiltrated opal and an inverse opal. Inverse opal-based photonic crystals offer several advantages over photonic crystals with opaline structures. Since, inverse opals have a robust continuous framework they benefit from more mechanical stability compared to opals. Inverse opals also have a better adhesion to the underneath support.[22,23]

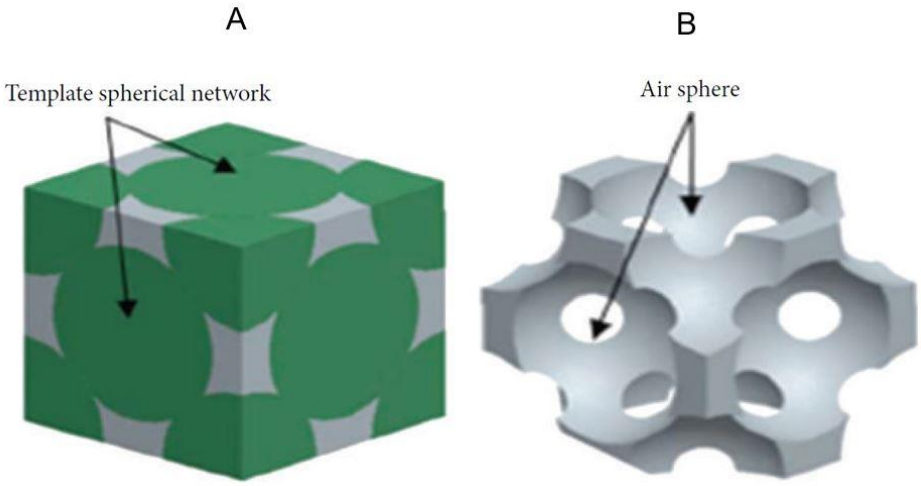

Figure 1.4. (A) Unit cell of an infiltrated opal, (B) unit cell of an inverse opal.
Photo is Reproduced with permission.[21]

Depending on the way of depositing the matrix, inverse opal fabrication methods can be categorized into two main approaches: self-assembly and co-assembly, see Fig. 1.5. In the self-assembly approach, template is first deposited and then matrix is infiltrated into the preassembled template, see Fig. 1.5 (A). This processes to make colloidal crystal films have typically resulted in the formation of cracks, colloid vacancies, and several other defects.

Capillary forces produced in the drying or infiltration step can lead to template cracking which is a major problem in the films obtained using this self-assembly/infiltration approach. Excessive and incomplete infiltration will also result in overlayer formation and structural collapse, respectively. Particle pre-sintering[24], changes in evaporative deposition conditions[25] are among the efforts that have been made to inhibit cracking and to increase the strength of these templates.[26]

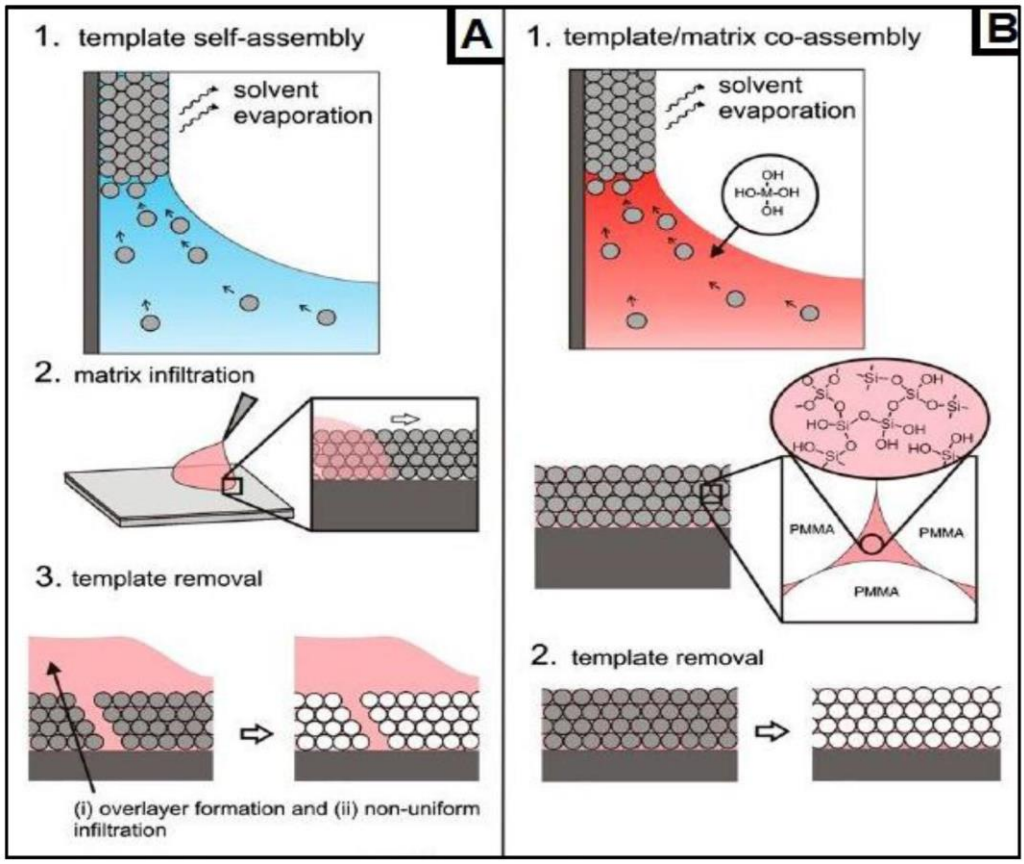

Figure 1.5. Two approaches for the fabrication of inverse opals: (A) self-assembly/infiltration (B) co-assembly.
Photo is Reproduced with permission.[26]

In the co-assembly approach (Fig. 1.5 (B)), the matrix and template are mixed and both are deposited onto the substrate simultaneously. Therefore, there is no need to infiltrate the matrix phase into the preassembled template in a separate step. Crack-free films have been produced using this method.[26]

1.4. Assembly methods

Based on the type of building blocks, the nature of external forces and the application of the resulting structure, different methods can be used to assemble colloidal particles into ordered arrangements.

Two methods which use centrifugal force to assemble particles are centrifugation and spin-coating. Centrifugation that is used in a tube has shown to be useful to make high quality bulk colloidal crystals.[27] Spin coating that is used on a surface, however, has

shown to produce patchy thin films since the force applied varies depending on the position of the film from the rotation centre.[28,11]

Another assembly method is vertical deposition in which a substrate is placed vertically in a colloidal suspension and the liquid meniscus goes lower as the liquid phase is evaporated gradually. This evaporation induces convective self-assembly of particles onto the substrate. This is a slow process as it takes several days for the liquid to completely evaporate. As this method is very sensitive to the conditions, such as temperature, humidity and concentration, during deposition, it is important to have a good control over these parameters in order to obtain a high-quality film.[29,11]

Dip coating is another technique for assembly of particles onto a substrate. Then, the substrate is pulled up or withdrawn from the suspension very slowly, inducing convective assembly of particles onto the substrate. This method is very similar to vertical deposition, since the substrate is vertically placed in the colloidal suspension. The thickness of the obtained film can be controlled by changing the speed of substrate withdrawal.[30,11]

The use of external magnetic field to assemble highly charged, paramagnetic colloidal particles has also been reported. This method has shown to be suitable for producing photonic crystals as these particles tend to self-assemble into ordered arrays. However, this method is only applicable to paramagnetic colloidal particles, which can be considered as a major limitation.[31,11,32]

Langmuir-Blodgett (LB) technique has also shown to be successful for assembly of colloidal particles. This is a two-step process in which a two-dimensional monolayer is first produced on a liquid surface, and in the second step, the monolayers are transferred onto a substrate and placed on top of each other in order to increase the film thickness and producing a 3D colloidal crystal.[33,11]

There are a number of other methods, such as sedimentation, electrophoretic deposition[34] and electrostatic interaction[35], which have also been reported for self-assembly of colloidal particles.

1.4.1. Sedimentation

Among all of the reported methods, sedimentation is the most basic and easiest one to use as the only driving force responsible for particle assembly is gravity. There is no need to use any complex equipment which makes it a low-cost method. Self assembly of colloidal particles by sedimentation involves two main steps as follows.

- In the first step, randomly distributed particles in colloidal dispersion sediment in a process which is explained by fluid mechanics. This process involves the balance of drag force, buoyancy and gravitational force. Stokes' law can be used to explain the drag force on the falling particles.[36] During this stage, other forces such as van der Waals forces (attraction), and electrostatic force (repulsive) between particles should also be considered.[37,38]

- In the second step, the particle deposition is completed resulting in a film with several layers in which a liquid (usually water) is present in the interstitial spaces between particles. This step is important in order to achieve a high quality film, since the solvent evaporation rate in this stage can strongly affect the quality of the obtained film. [38,39]

There are several factors that can influence the quality of a self-assembled colloidal crystal obtained by sedimentation. Relative humidity has been shown to play a vital role to produce an ordered crystal film. When the relative humidity is high, the evaporation rate is decreased, which reduces the shrinkage stress and results in subsequent cracks in the film. However, when the relative humidity is low, the evaporation rate is increased, resulting in a higher vertical growth rate and more internal stresses. This can severely affect the quality of the obtained film.[40,41,42]

Another factor which can directly affect the fabrication of self-assembled colloidal crystals by sedimentation is the temperature. It has been shown that temperature can have two effects on the uniformity of the resulting film. First, a high temperature speeds up the evaporation rate, which does not allow enough time for particles to arrange in a well-ordered structure. Second, when the temperature is high, particles have higher thermal energy which makes them move faster. Faster particle movements prevent the formation of a highly ordered structure. [42,43]

Concentration of particles in a colloidal dispersion also plays an important role in controlling the regularity of the obtained structure. A very low concentration results in a thin and sometimes patchy film. On the other hand, a very high concentration of colloids can also decrease the uniformity of the resulting film, since the amount of colloidal particles

settling toward the substrate is too much for a stable growth, which prevents formation of an ordered arrangement. [42,44]

The other factor influencing self-assembly of colloids during sedimentation is particle size. It has been reported that, as a result of slow movement of particles and their collisions, very large particles tend to have an unbalanced growth rate which consequently prevents formation of ordered structures. Too small particles also tend to form irregular films.[39,45]

Various drawbacks have been reported for self-assembly of colloidal particles using sedimentation such as vacancies, cracks, grain boundaries and dislocations which can limit their use in some applications. [44,46]

There are mainly three forces acting on each particle during sedimentation in a colloidal dispersion (Fig. 1.6). (1) force of gravity (F_g), which is a downward force attracting the particle toward the bottom of colloidal dispersion, (2) drag force (F_d), which is a force acting opposite to the direction of the particle moving relative to the surrounding fluid. During sedimentation, the particle is moving downward. Therefore, the drag force acting on the particle is upward, (3) buoyancy force (F_b), which is an upward force equal to the weight of the fluid displaced by the particle.[47]

Net force on the particle can be obtained by combining these three forces as follows:

$$F_{net} = F_g - F_d - F_b \qquad (1.1)$$

Force of gravity can be obtained by the following equations, in which m_p is the mass of particle, g is the acceleration of gravity, ρ_p is the density of the particle, V_p is the volume of the particle, and r is the radius of the particle.

$$F_g = m_p \mathrm{g} = \rho_p V_p \mathrm{g} \qquad (1.2)$$

$$V_p = \frac{4\pi r^3}{3} \qquad (1.3)$$

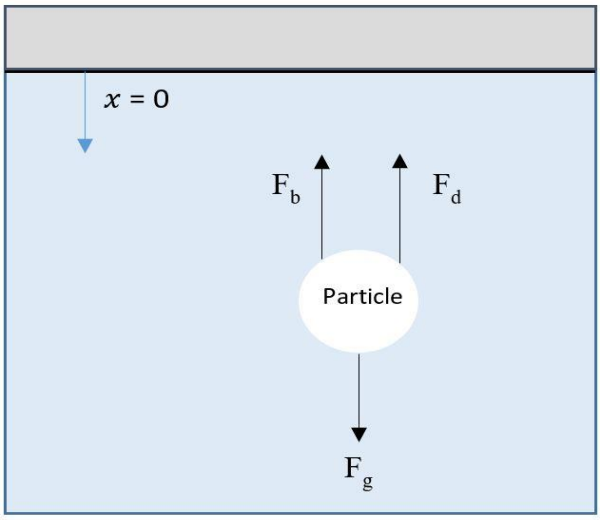

Figure 1.6. Schematic representation of the forces acting on a particle during sedimentation. The three forces are the force of gravity (F_g), drag force (F_d), and buoyancy force (F_b).

Moreover, the buoyancy force is shown as follows (ρ_f represents density of the fluid),

$$F_b = \rho_f V_p g \qquad (1.4)$$

The drag force equation is shown below[48], in which η_f and v are viscosity of fluid and velocity of the particle, respectively.

$$F_d = 6\pi\eta_f r v \qquad (1.5)$$

In this study, x would be considered as the distance off the top surface of the fluid, so the particle velocity term is given by the gradient of distance with respect to time.

$$v = \frac{dx}{dt} \qquad (1.6)$$

Based on Newton's second law of motion, one could calculate F_{net} as indicated below,

$$F_{net} = m_p a \qquad (1.7)$$

where the acceleration term (a), is also the gradient of velocity with respect to the time.

$$a = \frac{dv}{dt} = \frac{d^2x}{dt^2} \qquad (1.8)$$

Now, by substituting the acceleration term in equation (1.7), F_{net} would be rearranged as depicted below,

$$F_{net} = m_p \frac{d^2x}{dt^2} \qquad (1.9)$$

Inserting equations (1.9), (1.2), (1.4), and (1.5) into the equation (1.1) would result in

$$m_p \frac{d^2x}{dt^2} = \rho_p V_p g - 6\pi\eta_f \mathrm{r} v - \rho_f V_p g \qquad (1.10)$$

$$m_p \frac{d^2x}{dt^2} = V_p g \left(\rho_p - \rho_f\right) - 6\pi\eta_f \mathrm{r} v \qquad (1.11)$$

Substituting equations (1.3) and (1.6) into equation (1.11) will provide the equation below,

$$m_p \frac{d^2x}{dt^2} = \frac{4\pi r^3}{3} g \left(\rho_p - \rho_f\right) - 6\pi\eta_f \mathrm{r} \frac{dx}{dt} \qquad (1.12)$$

In order to solve the aforementioned equation, one can divide the entire equation by m_p, and rearrange,

$$\frac{d^2x}{dt^2} + \left(\frac{6\pi\eta_f \mathrm{r}}{m_p}\right)\frac{dx}{dt} - \frac{\frac{4\pi r^3}{3} g}{m_p} \left(\rho_p - \rho_f\right) = 0 \qquad (1.13)$$

For the sake of simplicity, the values of $\left(\frac{6\pi\eta_f \mathrm{r}}{m_p}\right)$ and $\frac{\frac{4\pi r^3}{3} g}{m_p} \left(\rho_p - \rho_f\right)$ are shown by α and β, respectively,

$$\frac{d^2x}{dt^2} - \alpha \frac{dx}{dt} - \beta = 0 \qquad (1.14)$$

To solve this second order differential equation, two boundary conditions needs to be satisfied. At t = 0, the position of the particle is zero, which means the first boundary

condition is $x(t = 0)$ = 0. The second boundary condition specifies at t = 0, the velocity of the particle is zero or $v(t = 0)$ = 0.

Now, by applying the above boundary conditions into the equation (1.14), one would be able to solve that differential equation to provide the following solution.[49]

$$x(t) = At + Be^{-Ct} + D \qquad (1.15)$$

where $A = \frac{\beta}{\alpha}$, B = $\frac{\beta}{\alpha^2}$, $C = \alpha$ and $D = -\frac{\beta}{\alpha^2}$.

Considering $m_p = 1.346 \times 10^{-16}\, kg$, $g = 9.8\ \left(\frac{m}{s^2}\right)$, r = $3 \times 10^{-7}\, m$, $\rho_f = 997\ \left(\frac{kg}{m^3}\right)$, $\rho_p = 1190\ (\frac{kg}{m^3})$, $\eta_f = 10^{-3}\ \left(\frac{kg}{\text{m.s}}\right)$ for PMMA particles suspended in water, the values of constants A, B, C, and D are $3.786 \times 10^{-8}\, s$, $9.012 \times 10^{-16}\, m$, $-4.202 \times 10^{7}\ (\frac{1}{s})$, -$9.012 \times 10^{-16}\, m$, respectively.

Based on the value of $x(t)$, or the distance travelled, the sedimentation time can be extracted from the equation (1.15). For a depth of 1 mm ($x(t) = 1\, mm$) the sedimentation time determined using equation (1.15) would be 9.5 hours.

1.5. Structural color

Light is reflected upon entering from a medium (e.g. air) to another (e.g. a solid). If the reflected light waves of a certain λ wavelength have constructive interferences, a color of that wavelength will appear which is called structural color[50] (Fig.1.7). This structural color is only sensitive to the change in the structure of a material rather than any chemical processes such as light absorption from colored dyes or pigments. In other words, the structural color of a photonic crystal is derived from light interference rather than light absorption. There is an interaction between the traveling light and interfaces of materials with different refractive indices. If these interaction sites have a periodicity and coherency on the wavelength-scale, as a result of constructive interference, a color with a specific wavelength will be appeared.[50] The structural color of a photonic crystal is due to the refractive index difference between the matrix and air which occupies the empty pore. The wavelength of the structural color can be described by the equation shown below[23]:

$$\lambda = 2D\ (n_{eff}{}^2 - \cos^2\theta_i\ )^{\frac{1}{2}} \qquad (1.16)$$

where λ is the wavelength of the reflected light, D is the distance between two planes of constructive interference, θ_i is the angle of incidence light and n_{eff} is the average refractive index of the photonic crystal. Based on equation (1.16), the wavelength of the structural color of a photonic crystal can be tuned by changing the mentioned parameters.[51] Structural coloration offers a number of advantages over conventional pigmentation including the ability to achieve a broad range of colors by changing the geometry of the material, producing permanent color without any photobleaching problem and the ability to utilize nontoxic materials to construct the photonic crystal.[52]

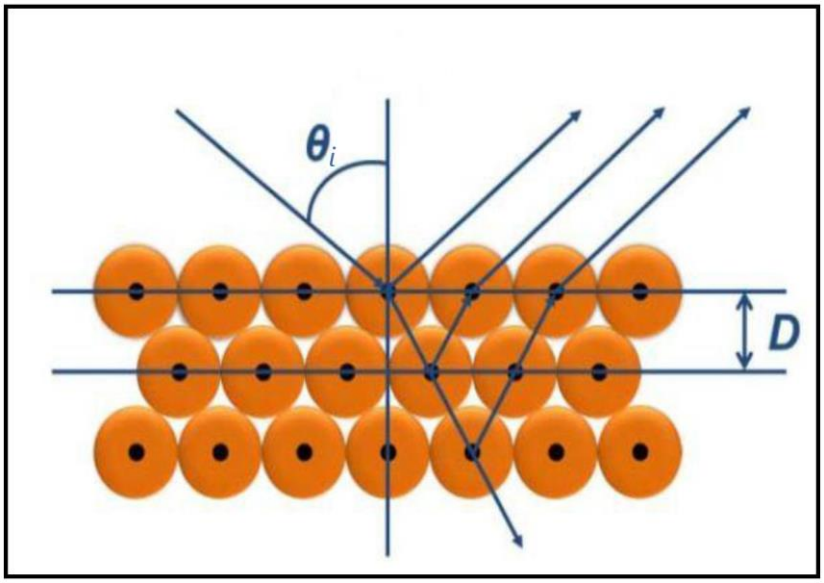

Figure 1.7. Schematic representation of light reflected from a photonic crystal
Photo is Reproduced with permission.[23]

1.6. Surface wettability

Surface wettability refers to the tendency of a surface to be wetted by a liquid and it can be evaluated by the contact angle that a liquid droplet forms on the surface. Contact angle, θ_C, (Fig. 1.8) can be determined by the force balance between surface tensions of liquid-vapor (γ_{LV}), solid-vapor (γ_{SV}) and solid-liquid (γ_{SL}) which is described by the Young's equation[53]:

$$\gamma_{LV}\cos\theta_C = \gamma_{SV} - \gamma_{SL} \qquad (1.17)$$

If the liquid droplet is water and $\theta_C \geq 90°$, the surface is called hydrophobic. For a water droplet forming $\theta_C < 90°$ the surface is called hydrophilic.[54]

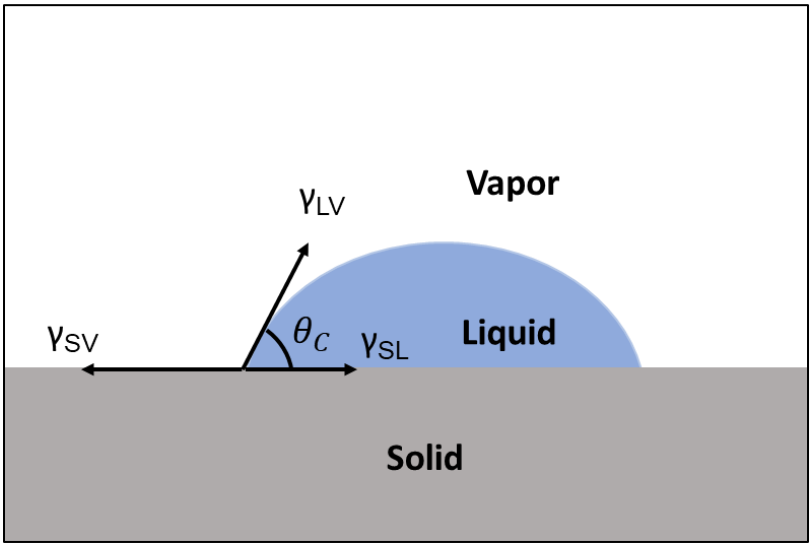

Figure 1.8. Schematic representation (not to scale) of balance of forces at an interface of liquid (L) vapor (V) and solid (S).

There are two factors which need to be considered when studying the wettability of photonic crystal films: (1) surface chemistry, (2) inter-pore geometry or neck angle. The photonic crystal film is considered to be wetted when the liquid is infiltrated into the pores. If the liquid is unable to penetrate the porous structure, the photonic crystal film will remain non-wetted.

1.6.1. Surface chemistry

Liquid infiltration into the pores of a photonic crystal can be controlled by applying a chemical coating on the surface of the pores. Alkylchlorosilanes are among the most common surface modifiers that have been reported for silica-based photonic crystals which can prevent liquid infiltration into the pores.[55,56] Fig. 1.9 schematically shows how the surface of silica is modified by an alkylchlorisilane. Depending on the structure of R group in the silane depicted in fig 1.9, the contact angle of a liquid on the silica surface can be tuned or increased. Liquids of lower contact angles are more likely to infiltrate pores of a photonic crystal whereas liquids with higher contact angles are less able to penetrate the pores.

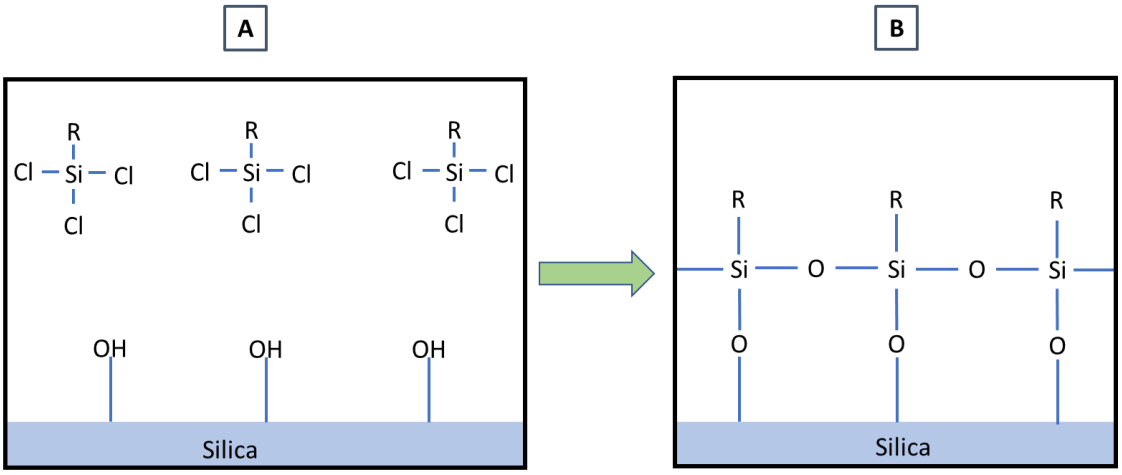

Figure 1.9. Schematic representation of silica surface modification; A) before silane treatment, B) after silane treatment.

1.6.2. Inter-pore Geometry

Inter-pore geometry is another factor influencing the wettability of the porous structure of photonic crystals. Photonic crystal films consist of multiple layers of pores and the pores in the upper and lower layers are connected through small inter-pore openings. These openings are called necks and they exhibit a re-entrant (or concave) curvature, see Fig. 1.10C. The curvature can be described by a term called neck angle, φ_0, which is defined as:

$$\varphi_0 = \sin^{-1}\frac{r_{neck}}{r_{pore}} \qquad (1.18)$$

where r_{neck} and r_{pore} are the radius of the neck and the pore, respectively (Fig. 1.10 (A)).[57] There is a force which prevents liquid infiltration into the pores of a photonic crystal which results from the re-entrant curvature of the necks. When the contact angle of a liquid on a flat substrate (with the same material as the photonic crystal matrix (Fig. 1.10 (B)) is smaller than the neck angle of photonic crystal, $\theta_C < \varphi_0$, the interfacial solid-liquid force exceeds the force barrier which lead to a wetting state (Fig. 1.10 (C)). On the other hand, If the contact angle of the liquid on a flat substrate is bigger than the neck angle, $\theta_C > \varphi_0$, a nonwetting state occurs, since the interfacial solid-liquid force is unable to overcome the force barrier (fig 1.10 (D).[56,58]

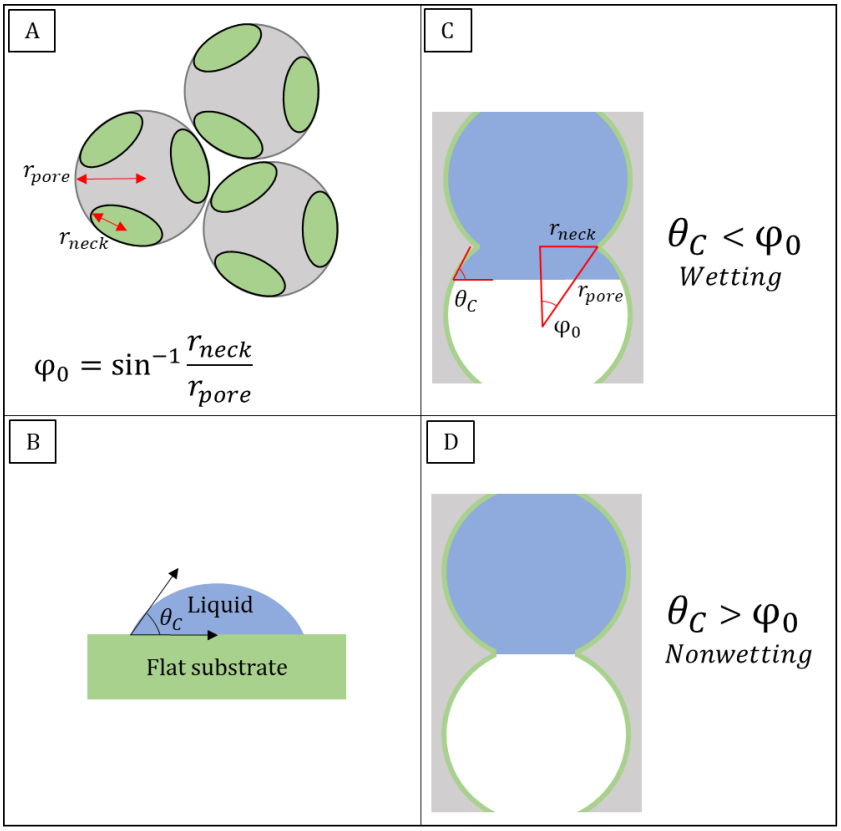

Figure 1.10. Wetting and nonwetting states in photonic crystal; A) Schematic representation of neck angle calculation, B) contact angle of the liquid on a flat substrate, C) wetting state occurs when contact angle is smaller than neck angle, D) nonwetting state occurs when contact angle is greater than neck angle.

1.7. Photonic crystals as chemical sensors

Photonic crystals have been used in various applications such as color displays, inks and paints, optical switches, lasers, filters, solar cells, and sensors.[4,1]

Photonic crystals with different compositions have been developed to be used as chemical sensors for sensing pH, solvent and etc.[23]

The refractive index difference between the matrix material (i.e. silica) and air (which occupies the empty nanopores) is related to the structural color of a photonic crystal film (PCF). The surface of the nano-sized pores inside the PCFs is typically coated by hydrophobic/oleophilic materials such as fluoroalkylchlorosilanes (FACS).[23,59] These coating materials will cause the pores wetted or not wetted by certain liquids (Fig. 1.11). When a liquid with a similar refractive index to the matrix wets the nanopores, the structural

color disappears due to the refractive index matching between the liquid and matrix (Fig. 1.11. (B)).

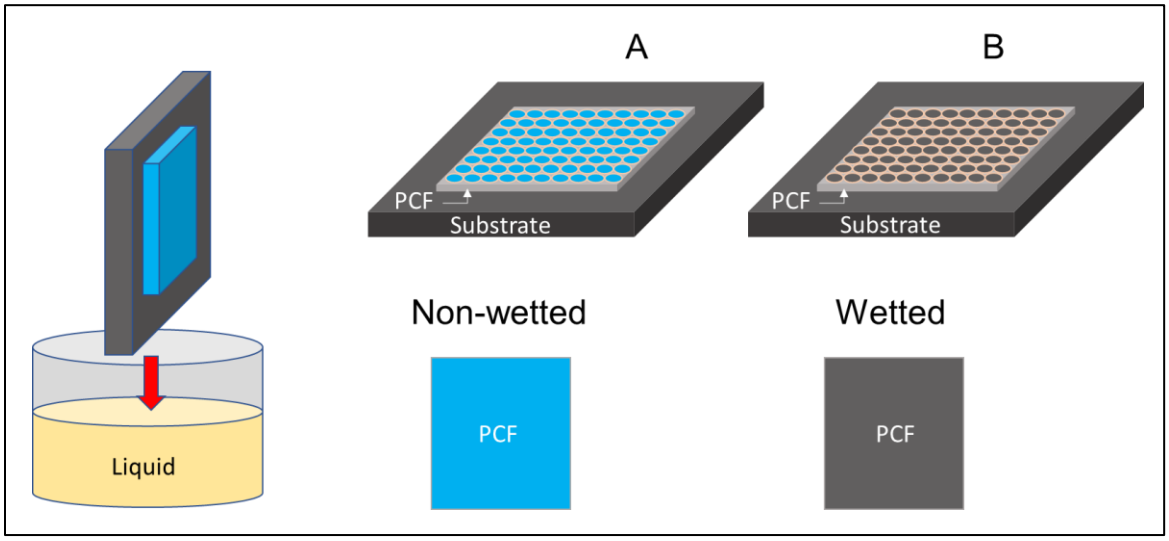

Figure 1.11. Sensing of liquid on PCF by wetting behavior; (A) Non-wetted PCF, (B) Wetted PCF.

The disappearance of the structural color provides a way to differentiate various liquids with different compositions based on the wettability of the nanopores.

A photonic crystal with structural color green can be seen in Fig. 1.12 Two different surface coatings are applied which are shown by red and yellow in the nanopores. When this photonic crystal is immersed in liquid 1, the red nanopores are not wetted by this liquid. The structural color is maintained in the region which is not wetted by this liquid. However, the structural color disappears in the areas which are wetted by this liquid. When this photonic crystal is immersed in liquid 2, a different pattern of color is produced. Using this mechanism, liquid 1 and liquid 2 can be differentiated by PCF.[50]

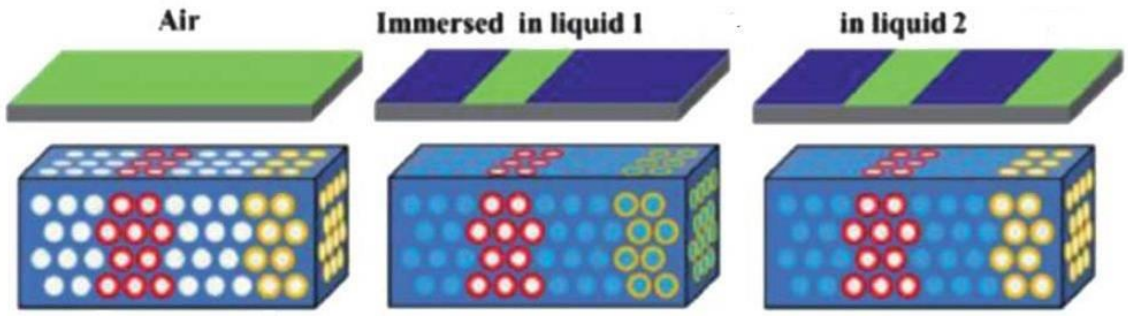

Figure 1.12. Two different chemical coatings ("red" and "yellow") used in a photonic crystal film differentiate liquids 1 and 2. Left: non-wetted PCF is green; middle: liquid 1 did not wet the pores treated with the "red" coating; right: liquid 2 did not wet the pores treated with both "red" and "yellow" coatings.
Photo is Reproduced with permission.[50]

Silica-based photonic crystal films with chemically functionalized nanopores offer a selective wettability threshold to differentiate liquids of different chemical compositions. There are two main approaches for liquid identification using photonic crystal films: (1) based on measuring color change of PCF due to the infiltration of a liquid with a different refractive index compared to air. In this approach, color changes may be small and angle-dependent, and this is complicated for non-trained persons to use. (2) based on color disappearance, in which colored (non-wetted) and dark (wetted) regions are observed, and this approach is easier to use as compared to the first approach.[50]

Aizenberg and her research team have developed photonic crystal sensors with patterned chemical coatings throughout their 3D porous structures. Patterning chemical functionalities in different regions on the sensor was achieved using oxygen plasma and removeable mask. Using this sensor, they have been successful to differentiate three pure liquids, such as isopropanol, acetone and water. They have also been able to differentiate water/EtOH mixtures of W50 , W22 (W22 is mixture of 22% water and 78% EtOH), W15 and W0.[58] In another work, they have been able to differentiate between water/EtOH mixtures of W10, W15, W20, W25 and W50.[60] The selectivity of their sensors has shown a remarkable improvement in another report. Applying new chemical gradients on their well-ordered photonic crystals, they have been able to differentiate between water/EtOH mixtures of W7.5, W5, W2.5 and W0 which have very small differences in surface tension. Various pure alcohols (e.g. methanol, ethanol and isopropanol) have also been differentiated using this sensor. Other than water/EtOH mixtures and alcohols, the

developed sensor has been used to differentiate between different pure alkanes (hexane, heptane, octane, nonane, decane) and different auto fuels (gasoline and diesel).[61] By replacing the conventional alkylchlorosilanes by a co-polymer based on a hydrophilic electrolyte monomer (acrylic acid) and a hydrophobic chromophore and applying different exposure times of ultraviolet (UV) light for photopolymerization, they could modify the wettability of the pores of the sensor and differentiate between water/EtOH mixtures of W100, W97.5, W95, W92.5, W90 and W87.5. The use of various exposure times of UV light for photopolymerization has been the key reason for their success to make the surface of the pores hydrophilic and consequently to differentiate between liquid mixtures with such a low difference in surface tensions.[62] In these reports of differentiating between water/EtOH mixtures, they did not manage to differentiate mixtures that have EtOH contents less than W50 (or 50% EtOH in water), possibly because of the inability to find a suitable chemical coating.

Sedighi and his colleagues have also developed dip-in sensors for differentiation of fuel mixtures with close chemical compositions. The wettability threshold for each sensor was tuned using a combination of different chemical coatings and neck angles. In this way, gasoline/EtOH mixtures of E10 (10% EtOH in gasoline), E5 (5% EtOH in gasoline) and pure gasoline have been differentiated by the sensor. The developed sensors have also been shown to be capable of differentiation of gasoline/oil mixtures with gasoline-to-oil ratios of 16:1, 20:1, 25:1, 32:1, 40:1, and 50:1 which are typical fuel/lubricant mixtures used in 2-stroke engines.[57]

1.8. Thesis objectives

Many methods reported to fabricate PCF have the inflexibility of building only one PCF on a substrate at a time. Therefore, different PCFs cannot be easily achieved on one single test strip. To overcome this inflexibility, the substrate will have to be diced into square pieces and assembled on a separate solid support to create a test strip, and this complicates the scale-up process in manufacturing. In this study, we wish to achieve the following objectives:

- We used evaporative sedimentation method to synthesis PCFs which brings about the advantage that we can have an array of PCFs on a single substrate.

- We performed parallel liquid mixtures analysis on several PCFs on the strips in order to multiplex the analysis of different liquid mixtures.

The reported method offers several advantages as follows:

- This way of constructing an array of PCFs on the same substrate will be less costly and more efficient as compared with other methods, since this will not require subsequent dicing and assembling of the different PCFs on a support.

- As compared with many other reported methods, the fabrication process of PCFs using this technique takes shorter time; from the manufacturing standpoint, this aspect makes our proposed method economically more efficient.

To understand the effect of the factor of neck angle on the wetting behavior of the PCF by a liquid mixture, a parameter was created to predict the behavior. This factor together with thickness and surface coating were studied as follows:

- Different concentrations of the matrix material and template were used to adjust neck angle and film thickness and further confirmed using scanning electron microscopy (SEM).

- The contact angles of several liquid mixtures when applied on a Si substrate coated with various surface coatings were measured. The differences in the contact angle values were used to tune the surface chemistry of the nanopores for differentiation of the mixtures which wet the pores of one PCF, but not others. Different surface coatings were used to tune the wettability of the pores.

The final sensor strip that consisted of an array of 6 PCFs was designed and created by using an optimized combination of neck angle, thickness and surface coating. The sensor strip has been shown to have the capability to differentiate between seven different liquid mixtures with a simple-to-read wetted/nonwetted platform.

Chapter 2.

Experimental section

Experimental methods, instruments and reagents used for this study are described in this chapter. Fabrication of polydimethylsiloxane (PDMS) mold, surface treatments including cleaning and functionalization, template/matrix preparation, sedimentation method and calcination are discussed in detail.

2.1. Materials and reagents

SYLGARD elastomer kit (SYLGARD 184) and silicone sealant 732 were purchased from Dow Corning Corp. (Midland, MI). Circular silicon wafers (4-inch diameter) were provided by UniversityWafer, Inc. (Boston, MA, USA). Poly (methyl methacrylate) (PMMA) nanospheres (1% solid content) with diameter of 318 ± 12 nm were purchased from Phosphorex, Inc. (Hopkinton, MA, USA). The PMMA nanospheres were suspended in deionized (DI) water. Tetraethyl orthosilicate (>99.0%) was obtained from Sigma-Aldrich (Oakville, ON, Canada). Trichloro(3,3,3-trifluoropropyl)-silane (3FS) was obtained from Sigma-Aldrich (Oakville, ON, Canada); nonafluorohexyltrichlorosilane (9FS) was provided by Gelest. Inc. (Morrisville, PA, USA); trichloromethylsilane (99%) (TMS) was purchased from Sigma-Aldrich (Oakville, ON, Canada); 3-(Trichlorosilyl)propyl methacrylate (TPMA) was obtained from Fluka (Buchs, Switzerland), with the chemical structures shown in Fig. 4.2. Dimethyldichlorosilane solution (2% w/v) in octamethylcyclotetrasiloxane (or Repel-silane) was purchased from GE Healthcare (Uppsala, Sweden).

The following solutions were prepared and used in this study:

- Piranha solution: Sulfuric acid (98%) and hydrogen peroxide (30%) were mixed in a 7:3 ratio. (Note: Piranha solution is very dangerous. It is a strong oxidizer and highly corrosive liquid upon contact with skin. It may result in explosion when mixed with organic materials).
- Sparkleen detergent: Sparkleen powder (10% w/v) was dissolved in DI water.

PDMS cleaning solution: The concentrated Liqui-Nox (Alconox, White Plains, NY) was diluted with DI water by a 1:10 ratio.

2.2. PDMS mold fabrication

Polydimethylsiloxane (PDMS) mold with 6 trenches was designed and created to fabricate an array of PCFs on a silicon substrate. PDMS is a hydrophobic, non-toxic and flexible polymer which can be sealed to a variety of solid materials such as glass, silicon and metal.[63] The steps to create PDMS molds were adopted from previous reports[64] and modified as follows:

1. Substrate Piranha treatment: A silicon wafer was cleaned with Sparkleen detergent followed by DI water. The silicon wafer was then immersed in 100 mL of piranha solution in a Pyrex dish (500 mL) in the fume hood for 1 h to clean the silicon surface and create hydroxyl groups on the surface to facilitate the subsequent silane coating. The wafer was then removed from the dish and was rinsed in water, ethanol (95%) and water, successively and was finally blow-dried.

2. Border formation on the wafer: In order to hold PDMS elastomer during the casting process, a circular border was formed on the wafer using silicone sealant 732 as shown in fig 2.1. (A). The wafer was then left for 24 h at room temperature for curing the silicone sealant.

3. PDMS casting and curing: PDMS elastomer base and curing agent in a 10:1 ratio was prepared. The mixture was kept in a freezer at -20 °C for 1 h so that air bubbles produced during mixing was removed. The surface of the silicon wafer was treated with Repel-silane (dichlorodimethylsilane) and was left for 15 min to be dried before PDMS casting. The PDMS mixture was then poured onto the silicon wafer to obtain a PDMS slab of 1 mm thickness and it was left at room temperature for 24 h to be cured.

4. PDMS peeling off and trimming: Using a knife blade, the edge of PDMS slab was cut and then the slab was peeled off gently from the silicon wafer. Six trenches, with dimensions of 2.5 mm width – 20 mm length – 1 mm depth, were cut using a knife blade on the PDMS slab (fig 2.1. (B)). The final PDMS slab was then washed with Liqui-Nox solution, blow dried, and stored for future use.

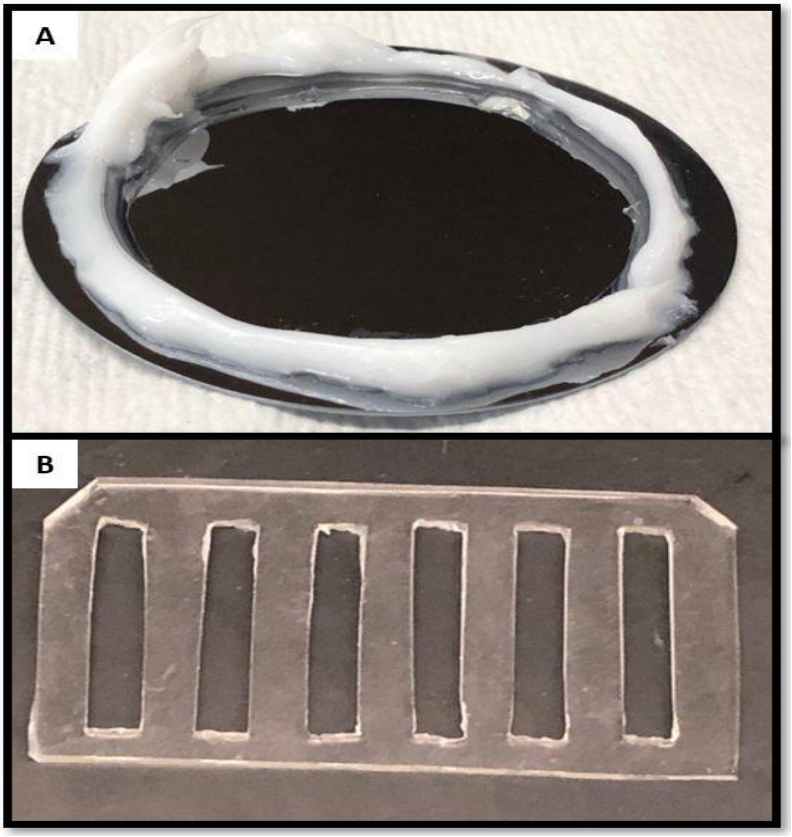

Figure 2.1. **(A) circular border formed on the wafer using silicone sealant (B) PDMS slab cut with six rectangular trenches (2.5 mm width – 20 mm length – 1 mm depth).**

2.3. Sealing PDMS mold with silicon substrate

Circular silicon wafers (4-inch diameter) were cut by a diamond glass cutter into two equal pieces, making two semicircles. After the semicircular silicon substrate was cleaned using Sparkleen detergent followed by rinsing with DI water, it was sealed to the PDMS mold (Fig. 2.2A). Then, the substrate was placed in a Pyrex dish containing 100 mL of piranha solution for 1 h to create a hydrophilic surface on the substrate. It was then removed from the dish and rinsed with water, ethanol (95%) and water successively and blow-dried.

2.4. PMMA-TEOS mixture preparation

A mixture of 0.01 M HCl, tetraethyl orthosilicate (TEOS) and anhydrous ethanol (EtOH) was prepared in a glass vial (a ratio of 1:1:1.5 w/w/w HCl/TEOS/EtOH) as the matrix. This solution was mixed thoroughly using a magnetic stirrer at 200 rpm for 1 h.

Poly (methyl methacrylate) (PMMA) nanospheres, which were suspended in water, acted as the template. The PMMA stock bottle was sonicated for 30 min to homogenize the colloids before use.

Aliquots of PMMA colloids and the matrix solution were added to a definite amount of DI water to form the PMMA-TEOS mixture in a tube. The mixtures were then capped and sonicated for 1 h.

2.5. PCF fabrication

In order to synthesize an array of silica-based PCFs, the PDMS mold consisting of six trenches was sealed on the silicon substrate (Fig. 2.2 and Fig 2.3(A)). The PMMA-TEOS mixture was then introduced into the trenches. This mold allows separate deposition of six different PMMA-TEOS mixtures on one silicon substrate without any leakage. After deposition of the PMMA-TEOS mixtures, the mold was placed in a covered plastic Petri dish in which the humidity was kept high (using wet tissues) to prevent any solvent evaporation. All samples were left in the plastic dish for 10-12 h to make sure the sedimentation of all nanospheres was completed. After sedimentation was completed, the cover was removed from Petri dish to start solvent evaporation. After 8-12 h, the silicon substrate, with the white-colored film deposited on its surface (Fig. 2.3(B)), was placed in a programmable oven for calcination. The oven temperature was ramped up to 500°C over 4 h, held at that temperature for 2 h, and ramped down to room temperature over 1 h. This calcination process caused thermal decomposition of the template (PMMA nanospheres) and conversion of TEOS to silica (SiO_2), forming the silica-based PCF. An array of several PCFs formed on the same substrate (Fig. 2.3(C)) was imaged by a smartphone camera at a viewing angle of 55°.

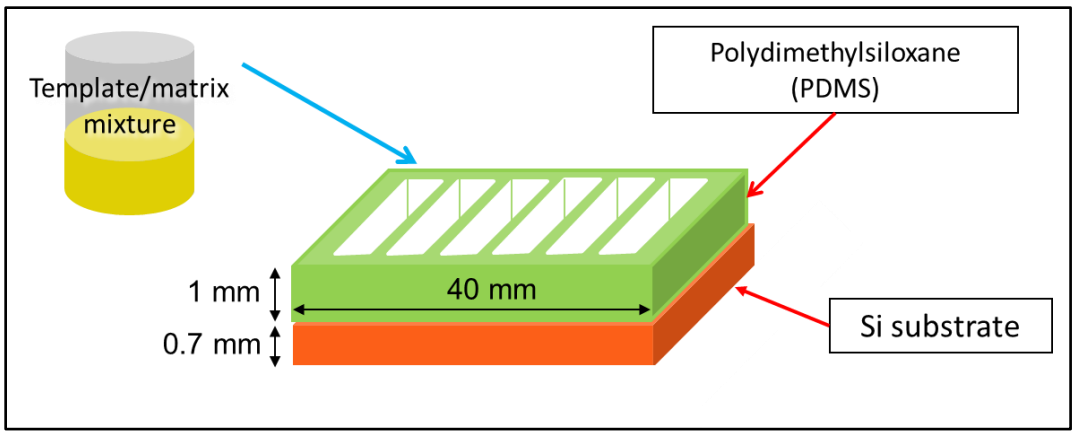

Figure 2.2. **Schematic representation (not to scale) of template/matrix mixture and PDMS mold consisting of six trenches sealed on Si substrate.**

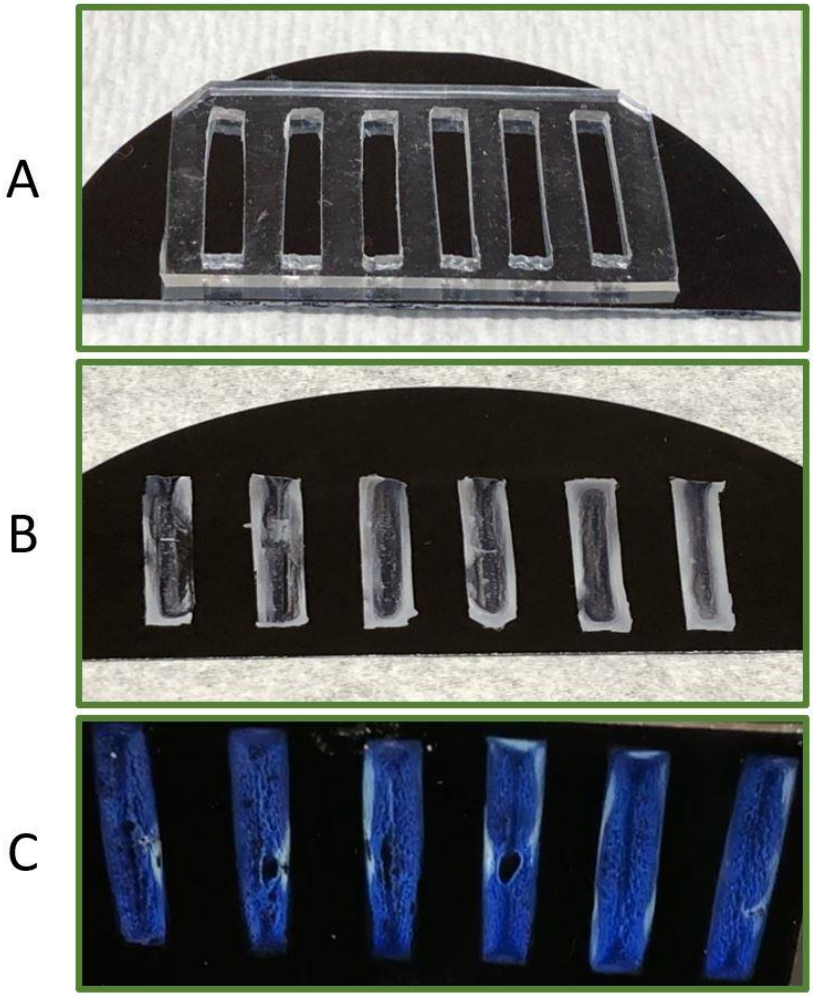

Figure 2.3. **Steps of PCF fabrication (A) sealing the PDMS mold to the silicon substrate, (B) six white-colored strips formed after drying, (C) an array of six blue PCFs was synthesized on the silicon substrate.**

2.6. Theoretically required amount of TEOS

The calculation for the number of PMMA particles (318 nm diameter) required to obtain a complete monolayer is given in appendix D. For a trench of area of 50 mm^2 (2.5 mm width – 20 mm length), the number of particles is 5.49×10^8. The volume of a monolayer is $1.6 \times 10^{-2}\ mm^3$.

The required amount of silica (SiO_2) which acted as the matrix to fill the interstitial spaces between the particles for one complete layer would be calculated by finding the 26% of the volume of one monolayer PMMA, since the packing density of face-centered cubic (FCC) structure is 74%.[14] Based on the volume of a PMMA monolayer in each trench ($1.6 \times 10^{-2}\ mm^3$), the amount of silica required to fill the interstitial space was calculated to be $4.1 \times 10^{-3}\ mm^3$. Considering the density of silica (2.65 g/cm^3)[65], the mass of silica required for one monolayer was calculated to be 9.1 µg.

The silica was obtained from a reaction of $Si(OC_2H_5)$ (TEOS) and water as shown below:

$$Si(OC_2H_5)_4 + 2H_2O \longrightarrow SiO_2 + 4C_2H_5OH \qquad (2.1)$$

The theoretically required amount of TEOS for reaction to obtain 9.1 µg of silica would be calculated using the molar mass of TEOS (208 g/mol), the density of TEOS solution (0.933 g/mL), and molar mass of silica (60 g/mol). Hence, the theoretically required amount of TEOS was calculated to be 0.034 µL.

2.7. Surface modification

In order to tune the surface chemistry of the pores, the silicon substrates were placed in a vacuum desiccator (Fig. 2.3), exposing PCFs on them to chemical vapors of a silane. For this purpose, two small vials containing 90 µL of a silane solution were placed into the desiccator. Trichloro(3,3,3-trifluoropropyl)-silane (3FS), nonafluorohexyltrichlorosilane (9FS), methyltrichlorosilane (99%) (TMS), 3-(trichlorosilyl) propyl methacrylate (TPMA) were the silanes used in this study. A vacuum suction was applied to the desiccator for 3-5 min and the PCFs were left exposed to the chemical

vapors inside the desiccator for 24 h. After chemical vapour deposition, the PCFs were baked at 150 °C for 20 min.

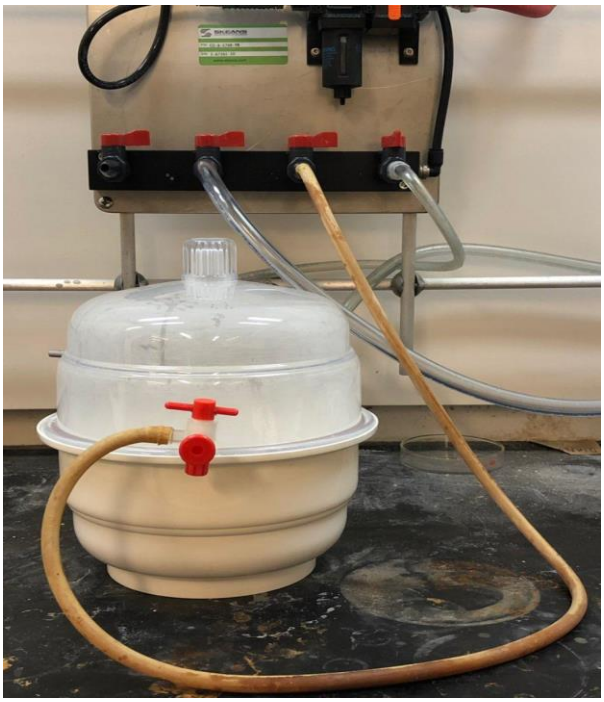

Figure 2.4. Chemical vapor deposition set-up including a vacuum desiccator, connecting tubes and vacuum suction apparatus.

The abovementioned procedure was also used for coating flat silicon substrates to measure contact angles of various liquid mixtures on different surface coatings.

2.8. Contact angle measurements

In order to quantify the wettability of various liquid mixtures on solid surfaces with different chemical coatings contact angle measurements were performed using a contact angle goniometer (OCA 15) manufactured by Data Physics Corp (San Jose, CA, USA). Using a micropipette, a small droplet of liquid (10 µL) was placed on the flat coated silicon substrate and the angle between the solid-liquid interface (SL) and liquid-vapor (LV) interface was measured.[66] Fig 2.4 shows a 10-µL droplet of a water/EtOH mixture (20% EtOH in water) on a flat silicon surface coated with 3FS. The value of θ_C shown in Fig. 2.4 is the contact angle of this liquid on the coated silicon surface.

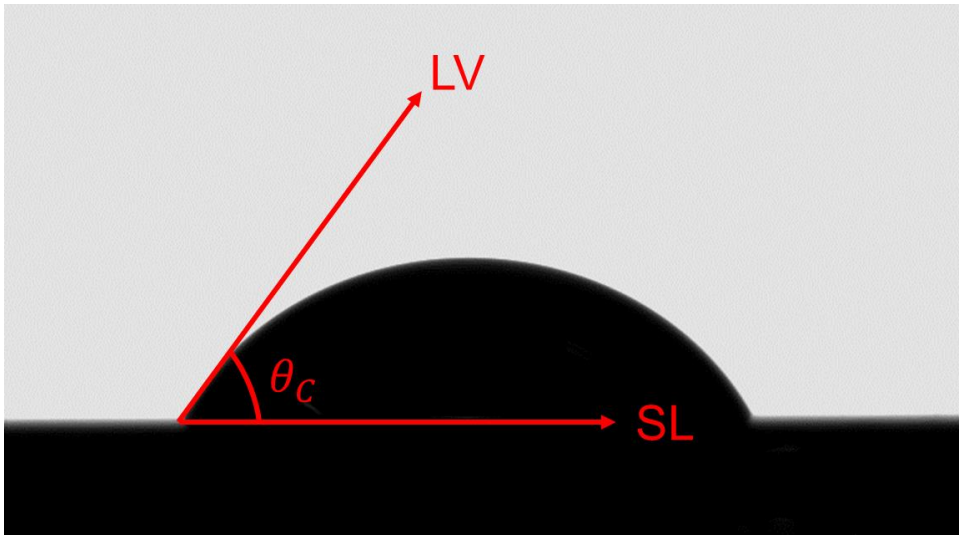

Figure 2.5. A 10 µL droplet of water/EtOH mixture (20% EtOH in water) on a flat silicon substrate coated with 3FS, θC is the contact angle of the liquid on the surface, LV is the liquid-vapor interface, and SL is the solid-liquid interface.

2.9. Scanning Electron Microscopy measurements

The scanning electron microscope (SEM) is a tool which has been used to get information on the morphology and size of a sample. The surface of the sample is scanned using a focused beam of fast moving electrons.[67]

In order to prepare samples for SEM imaging to prevent charge build-up[67], they were coated with a thin layer of conductive iridium using a Carbon & Iridium Coating System (EM ACE600) by Leica (Wetzlar, Germany). Coating was achieved by a magnetron sputter by producing ionized argon which eroded the target material (iridium) in a plasma state. Sputtering was performed at a high vacuum (10^{-5} Torr) for about 1 min to attain a layer of iridium with a thickness of 10 nm.

After sample preparation, SEM measurements with a voltage of 15 kV to accelerate electrons were carried out using the Nova NanoSEM 430 system manufactured by FEI (Hillsboro, Oregon, USA). Except cross-sectional images which were taken without any tilt (0°), many of the SEM images in this work were taken with a tilt of 40°. The working distance (WD) was set 5 ± 1 mm for all the samples.

2.10. Measurement of reflectance spectra

Reflectance spectroscopy shows the relation between the intensity of an incident light with the intensity of the reflected light as a function of wavelength. Reflectance measurements can provide information on the color of a sample.

Reflectance spectra were measured using a fiber optic spectrometer (SD2000) by Ocean Optics (Largo, FL, USA). For the reflectance measurements, the substrate was tilted 55°, in order to obtain sharp peaks as the color reflected from the fabricated PCFs were angle-dependent.

2.11. Optical imaging

Optical images were taken using a 12MP smartphone camera (iPhone X), Apple, Inc (Cupertino, CA, USA). Optical images of photonic crystal films were taken at an incidence angle of ~55 degrees.

2.12. Wetting tests

After fabrication of the PCF samples, they were checked by the water wetting tests. After each sample was immersed in water, the blue structural color should disappear due to liquid penetration into the pores, and the color of the PCF should reappear after blow-drying the sample with compressed air. These samples were thus tested to verify that the pores of the PCFs are well ordered without any blockings.

The samples were then coated and wetting tests were performed with various water/EtOH mixtures. The wetting tests were started with W5 and continued to W100 (pure water) with an increment of 5% water in water/EtOH mixtures. In order to be consistent, each sample was left immersed in water/EtOH mixtures for 10 sec. The samples were blow-dried by compressed air after each wetting test in order to speed up the color recovery needed for the subsequent wetting tests.

In order to investigate the effect of chemical coating on the wetting behaviour of PCFs without the influence of the PCF structural factors, one single PCF sample was used. After performing all the wetting tests for a specific coating on the PCF sample, the

coating was thermally removed. This was achieved by placing the sample in a programmable oven, with the temperature ramped up to 800°C over 8 h, held at 800°C for 1 h, and ramped down to room temperature over 3 h. In order to confirm complete removal of the coating, the sample was verified by a water wetting test. The removal of the coating was verified by the disappearance of the structural color of the PCF upon its immersion in water.

Chapter 3.

Optimization of PCF fabrication

In this chapter, we optimize the conditions for fabricating uniform PCFs that show a bright structural color in order to be used in our final sensor. There are various factors that can influence the structure of PCFs, including template/matrix ratio, deposition method, sedimentation time and solvent evaporation rate. These factors, which all have effects on the film uniformity and hence on the resulting structural color of the obtained PCFs, are discussed in detail.

3.1. Characterization of fabricated PCF

Fig 3.1 (A) shows the optical image of a PCF fabricated with the amounts of PMMA, TEOS and water to be 35 μL, 3 μL, 1010 μL, respectively. The cross-section SEM image of the sample (Fig. 3.1 (B)) shows that the fabricated PCF is made up of 3 layers, and this is consistent with our theoretical calculations (see Appendix D). Fig. 3.1 (C) and (D) show the top-view SEM images of the fabricated PCF in two different magnifications. A honeycomb-like structure is observed from the SEM images which show a periodically ordered arrangement of nanopores.

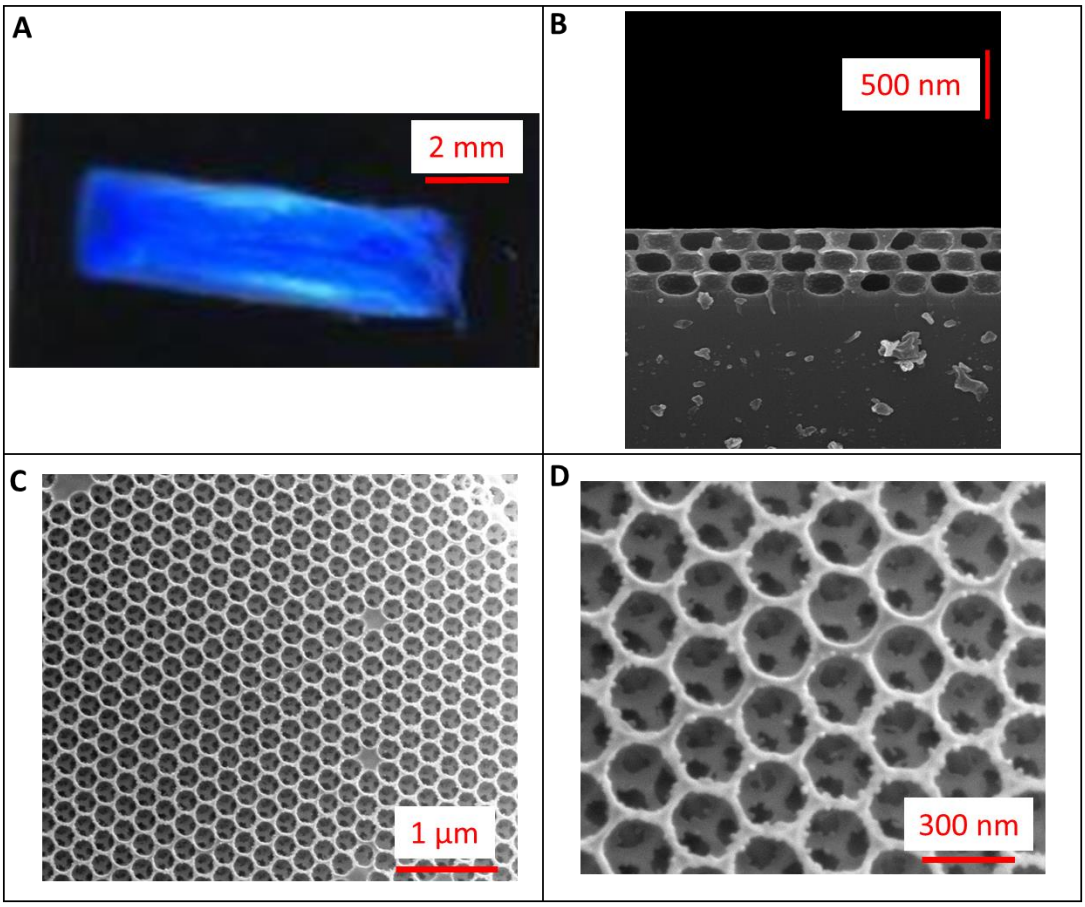

Figure 3.1. **(A) optical image of PCF showing a blue structural color on the film, (B) cross-section SEM image of the PCF which consists of 3 layers, (C) top view SEM image of the PCF with a magnification of 30,000 times, (D) top view SEM image of the PCF with a magnification of 100,000 times.**

Fig 3.2 shows the reflectance spectrum of the same PCF in the visible region. Reflectance (R) is defined as the reflection intensity divided by the incident intensity. Based on the reflectance spectra, there is a peak around 430 nm which contributed to the blue color. Therefore, the reflectance spectrum confirms that the structural color of the fabricated PCF is blue. As discussed in chapter 1, the wavelength of the reflected light of a PCF can be derived from equation (1.16) using the values for D and θ of 190 nm and 55°, respectively. The average refractive index (n_{eff}) was determined by using the refractive indices of silica and air of 1.475[68] and 1.0[69], respectively, the matrix of 53% ± 6% and the void of 47% ± 6% (see appendix E) to give a value of 1.252 ± 0.025. Therefore, the wavelength of reflected light for this PCF was calculated to be 423 ± 10 nm, which is consistent with our reflectance spectrum results.

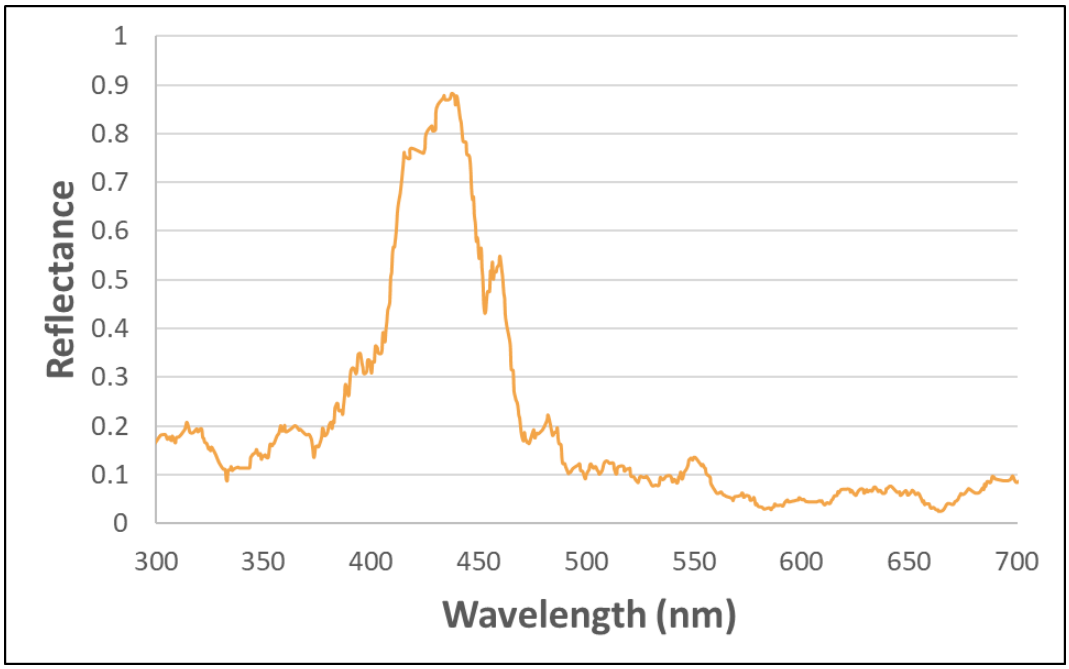

Figure 3.2. Reflectance spectrum of a fabricated PCF showing the reflected light with a peak in the blue region of visible light.

3.2. Advantage of template/matrix co-assembly advantage over template self-assembly/matrix infiltration

In this section, two different methods for the deposition of template and matrix have been performed and compared.

Method A was the template self-assembly/matrix infiltration approach. To fabricate this sample A, a mixture of PMMA and water was prepared using 50 µL of PMMA and 850 µL of water. A volume of 100 µL of this mixture was deposited in each trench. After the PMMA particles were dried, 0.22 µL of TEOS was infiltrated to fill the interstitial spaces between the PMMA particles.

Method B was the template/matrix co-assembly approach. For preparation of this sample B, a mixture of PMMA (50 µL), TEOS (2 µL) and water (850 µL) was prepared. A volume of 100 µL of this mixture was deposited in each trench to produce six PCFs.

Based on the number of PMMA particles, PCFs were designed to consist of 5 layers in both samples. In the template self-assembly/matrix infiltration approach, template particles are first deposited in the trenches followed by drying, see Fig. 3.3 (A) (i). In the second step, the matrix is infiltrated into the preassembled template particles, see Fig. 3.3 (A)(ii). Fig. 3.3 (A)(iii) shows the optical image taken after the template and matrix were dried. The calcinated PCFs are shown in Fig. 3.3. (A)(iv). The PCFs fabricated using this method are not uniform without a bright structural color which can be attributed to segregation of silica during solvent evaporation. In the template/matrix co-assembly the template and matrix were deposited simultaneously and dried, see Fig. 3.3 (B)(i). After calcination, the PCFs showed a high degree of uniformity with a bright blue structural color, see Fig 3.3 (B)(ii).

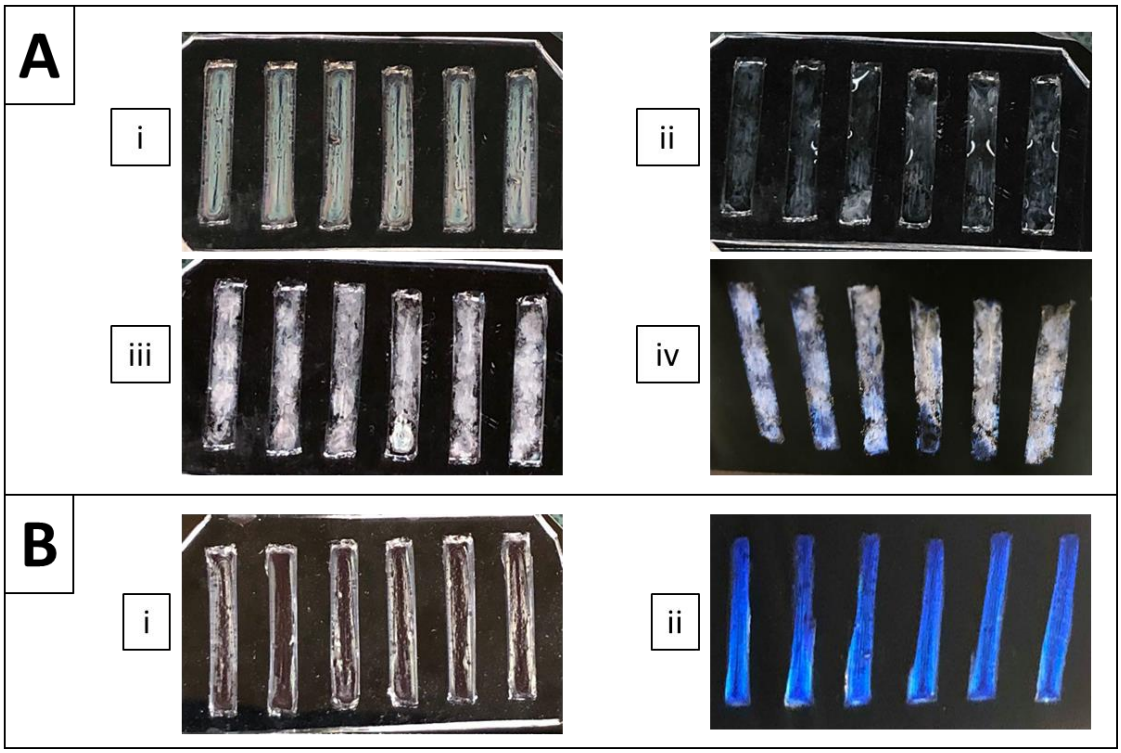

Figure 3.3. **Two different template/matrix deposition methods for PCF fabrication; (A) template self-assembly/matrix infiltration, i) PMMA templates are deposited and dried, ii) TEOS solution is infiltrated into the pre-assembled PMMA templates, iii) PMMA templates and TEOS solution are dried, iv) sample is calcinated, (B) template/matrix co-assembly (sedimentation time and evaporation rate were 9 h and 12.5 µL/h, respectively), i) PMMA-TEOS mixture is deposited and dried, ii) sample is calcinated exhibiting a blue structural color.**

The template/matrix co-assembly has been shown to be a more suitable method to produce uniform PCFs with strong structural color as compared with template self-assembly/matrix infiltration.

3.3. Effect of sedimentation time on PCF quality

In this section, we study the effect of sedimentation time on the quality of PCFs. The amounts of PMMA, TEOS and water used were 30 µL, 2 µL and 850 µL, respectively, to achieve PCFs with 3 layers. Sedimentation times of 1, 5, 9 h were used to fabricate three PCFs. Samples were dried with the same evaporation rate of 12.5 µL/h. As it can be seen in Fig. 3.4, by increasing the time of sedimentation, the quality of PCFs is improved. Sample with a sedimentation time of 9 h showed uniform PCFs with a bright structural color which is consistent with our theoretical calculations for the time needed for a complete sedimentation (see section 1.4). Based on Fig. 3.4 (A) and (B) PCFs produced with sedimentation time of 1 and 5 h are non-uniform with noticeable patchy areas.

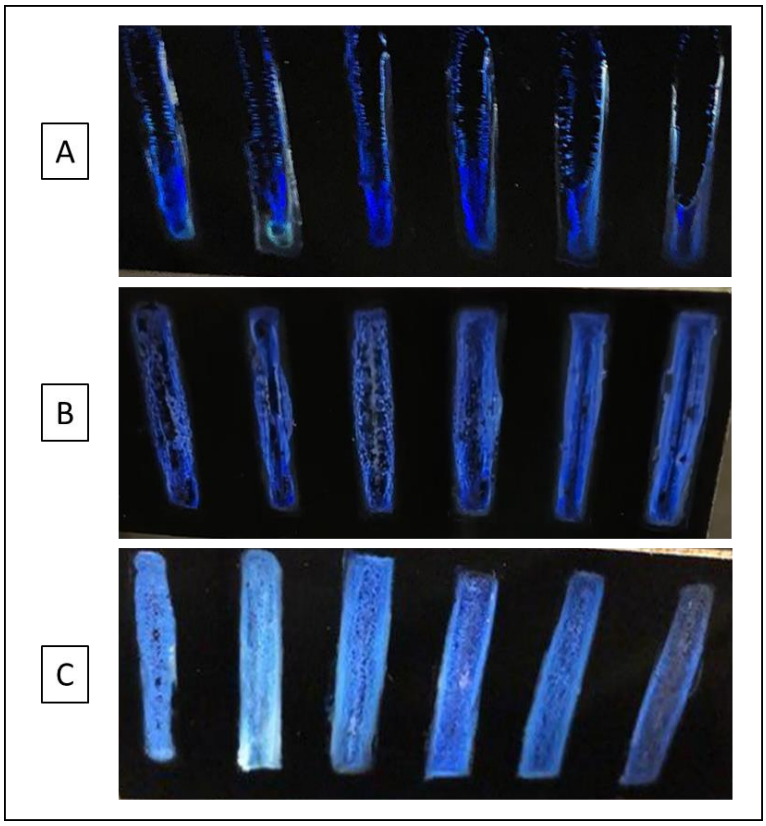

Figure 3.4. Effect of sedimentation time on the quality of PCFs: (A) 1 hours (B) 5 hours (C) 9 hours.

The non-uniformity observed for these two samples can be due to the fact that PMMA particles were not given enough time for a complete sedimentation. As a result, the evaporation step was started before the sedimentation step was completed which might have prevented the formation of an ordered arrangement of PMMA particles.

3.4. Effect of evaporation rate on PCF quality

In this section, the effect of evaporation rate on the structure of the PCF is investigated. The amounts of PMMA, TEOS and water used were 40 µL, 3.5 µL and 850 µL, respectively to achieve PCFs. As it is shown in Fig. 3.5, three samples with different evaporation rates were produced and the sample dried with an evaporation rate of 12.5 µL/h (Fig. 3.5C) showed higher uniformity with a bright structural color. Samples which were dried faster showed cracks and patchy areas. The higher the evaporation rate, the higher the possibility of destroying the packing arrangement of PMMA particles.

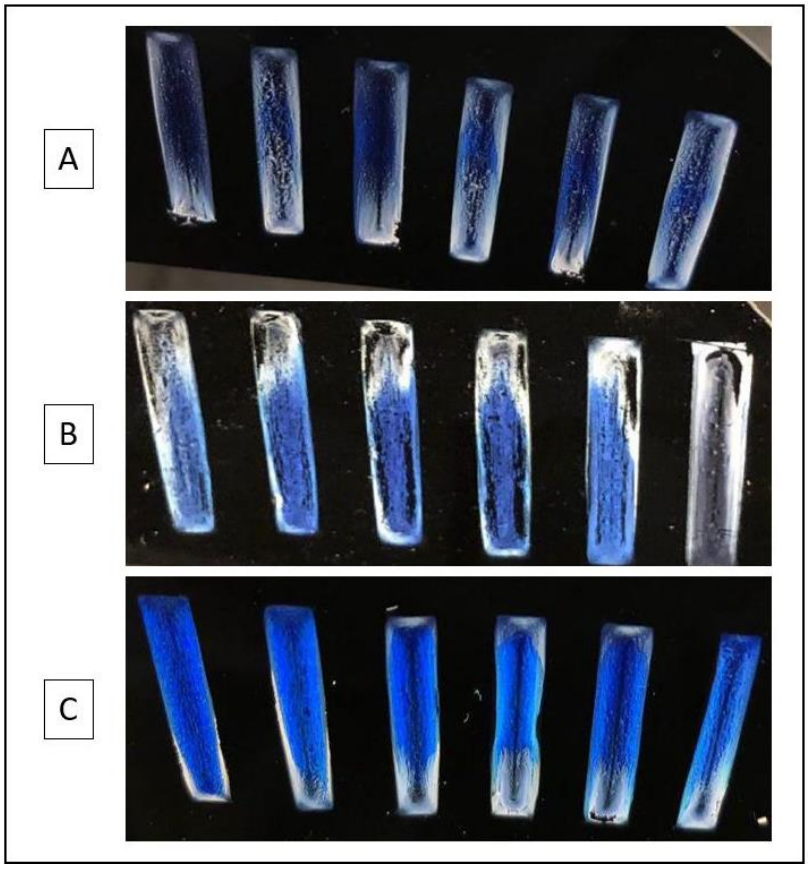

Figure 3.5. Effect of evaporation rate on the quality of PCF. The humidity was controlled in such a way that evaporation rate was: (A) 50 µL/h, (B) 25 µL/h, (C) 12.5 µL/h.

3.5. Effect of TEOS/PMMA ratio on PCF quality

In this section, the effect of TEOS/PMMA ratio on the quality of a PCF is investigated. PMMA and water of 30 µL and 860 µL, respectively, were used to achieve PCFs with 3 layers. Fig. 3.6 shows the change in the quality of a PCF by increasing the ratio of TEOS/PMMA. For the PCFs with TEOS/PMMA ratio of 0.08 and 0.12, the amount of TEOS seems insufficient to make full layers. For the PCFs with TEOS/PMMA ratio of 0.16 and 0.18, the amount of TEOS seems to be excess since there are areas with white colors which shows the segregation of silica. The optimum ratio of TEOS/PMMA was found to be 0.14 for these PCFs, which was produced using 4.2 µL and 30 µL of TEOS and PMMA, respectively. Based on the results obtained in this chapter, sedimentation time, evaporation rate and TEOS/PMMA ratio of 9 h, 12.5 µL/h and 0.14, respectively, were observed to be the optimum conditions for making a high quality PCF with 3 layers.

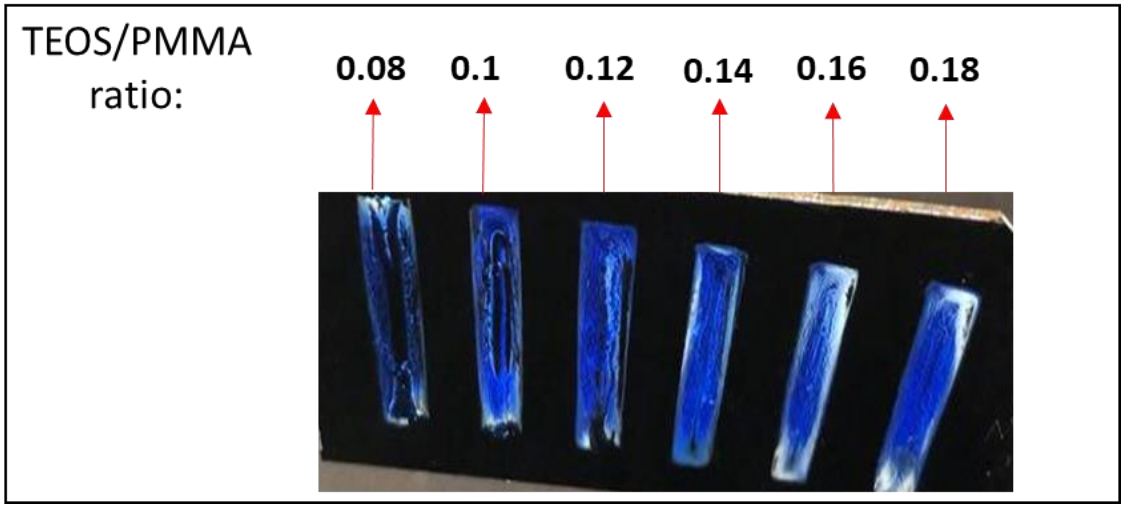

Figure 3.6. Effect of TEOS/PMMA ratio on the quality of PCF.

Chapter 4.

Interfacial properties of water/EtOH mixtures

In this chapter, the interfacial properties of various water/EtOH mixtures on 4 different coatings are investigated. Trichloro(3,3,3-trifluoropropyl)-silane (3FS), nonafluorohexyltrichlorosilane (9FS), trichloromethylsilane (TMS) and 3-(trichlorosilyl)propyl methacrylate (TPMA) are 4 chemical compounds used to provide surface coatings used in this chapter.

Table 4.2 shows the measured contact angles of various water/EtOH mixtures on flat silicon substrate that was coated with TPMA, TMS, 3FS and 9FS. The water/EtOH mixtures are given by the percentage of water, shown by the number after the letter “W”. For example, W60 is mixture of 60% water and 40% EtOH. In Fig. 4.1 the contact angles of W100, W80, W60, W40, W20 and W5 on flat silicon surface coated with TPMA, TMS, 3FS and 9FS are plotted. Based on Fig. 4.1, as the water contents of these mixtures decrease, the contact angles decrease. Since water (72.01 mN/m at 25° C) has a higher surface tension as compared to EtOH (21.82 mN/m at 25° C), the higher contact angles of pure water (W100) on a coated surface as compared with other mixtures of lower EtOH content are resulted from the higher surface tension of water. In other words, as the water content decreases in the water/EtOH mixtures, the surface tension of the whole mixture decreases which lead to a lower contact angle.

Table 4.1. **The measured contact angles from 6 different water/EtOH mixtures on flat silicon substrate when coated with: 9FS, 3FS, TMS, and TPMA. SD represents the standard deviations of three measurements.**

Water/EtOH mixture	TPMA	SD	TMS	SD	3FS	SD	9FS	SD
W100	39.8	0.9	54.1	0.2	70.8	0.4	87.6	1.5
W80	33.4	0.7	49.0	0.7	59.7	1.0	71.5	1.6
W60	22.9	1.7	33.7	0.3	41.1	1.0	53.1	1.1
W40	12.7	1.3	24.5	1.4	32.3	2.0	42.5	1.2
W20	7.4	0.5	15.4	0.5	22.1	1.3	30.8	1.0
W5	6.0	0.8	7.4	0.2	12.5	0.2	13.7	1.4

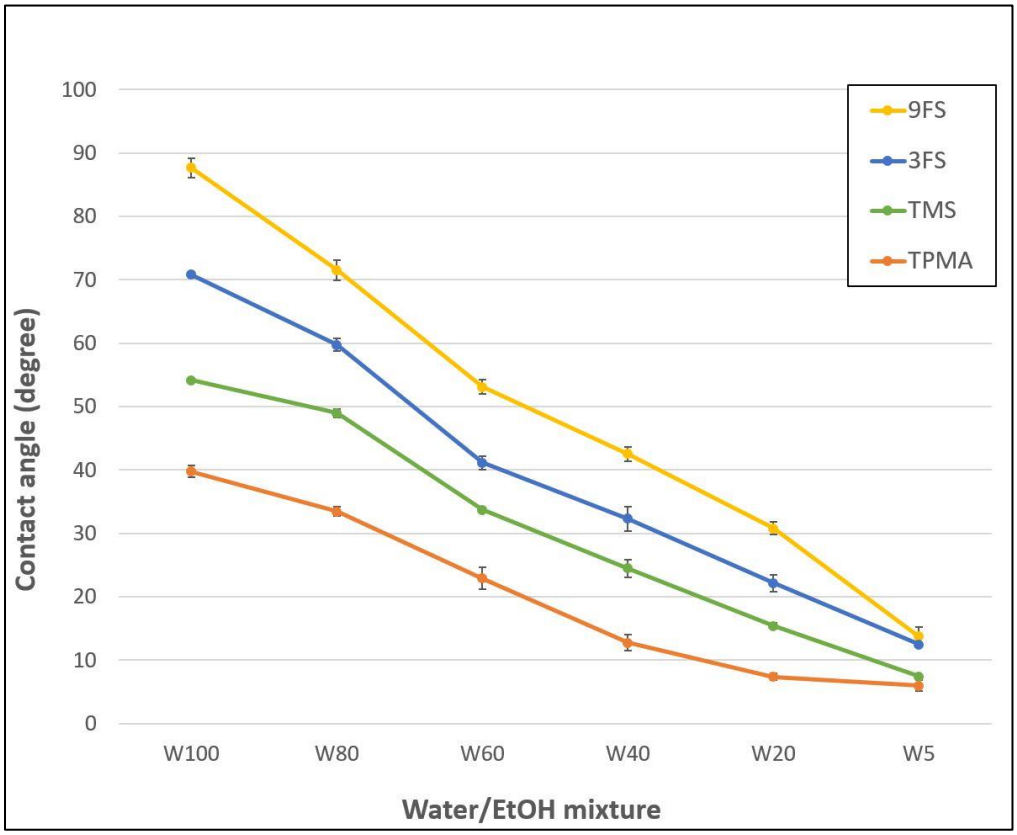

Figure 4.1. **The measured contact angles from 6 different water/EtOH mixtures on silicon substrate when coated with; 9FS , 3FS, TMS, and TPMA.**

From Fig. 4.1 the value of contact angle for a specific water/EtOH mixture on 9FS coated silicon is higher than that on 3FS. This indicates 9FS is more hydrophobic than

3FS; in order to justify the higher hydrophobicity of 9FS as compared to 3FS, their molecular structures should be considered. Fig. 4.2 shows the molecular structure of TPMA, TMS, 3FS and 9FS. Based on Fig. 4.2, The high hydrophobicity of 9FS comes from a strong force within 9FS and hence low interaction between 9FS and the liquid. TPMA shows to be a more polar molecule compared with TMS as a result of presence of two carbon-oxygen bonds in its molecular structure. Therefore, TPMA has a lower hydrophobicity compared to TMS, producing lower contact angle values. TPMA and TMS both have lower hydrophobicity compared to 3FS and 9FS based on the obtained contact angles of water/EtOH mixtures on these chemical coatings. As a result, TPMA, TMS, 3FS and 9FS have increasing hydrophobicity. The contact angle values of water/EtOH mixtures obtained on TMS and 3FS are in a good agreement with an earlier reported work.[58]

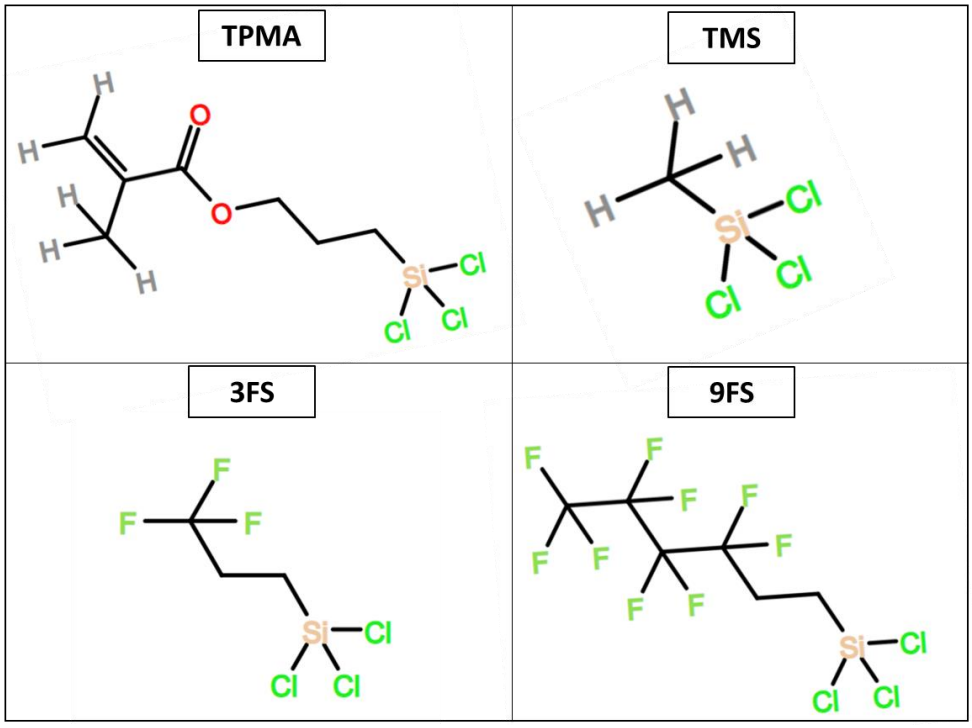

Figure 4.2. schematic molecular structure of TPMA, TMS, 3FS and 9FS.

The contact angles of various gasoline/oil mixtures on flat silicon substrates coated with 3FS and 9FS were also measured (see appendix A). However, the values of contact angles for six gasoline/oil mixtures of 16:1, 20:1, 25:1, 32:1, 40:1 and 50:1 (the ratio of gasoline to oil is 50 to 1) on a single coating did not show any noticeable difference. Since

the contact angle difference in water/EtOH mixtures was wider as compared to gasoline/oil mixtures, we chose to explore the former set of mixtures in subsequent chapters.

The contact angle of gasoline/oil mixtures over time was also measured and plotted (see appendix B). Changes of contact angles with time are not high for involatile liquids such as water and oil. However, for volatile liquids such as gasoline, the decreases in contact angles occur over a time of 60 sec, probably due to a change in the shape of the liquid droplet. So, the contact angle measurements were fixed at a time of 1 sec after dispensing the liquid droplet.

Chapter 5.

Parameters affecting wetting behaviour of a PCF

In this chapter the effect of neck angle, chemical coating and film thickness on the wetting behaviour of PCFs by various liquid mixtures are investigated. Then, a combination of these three factors are used to tune the wettability of the PCFs, and a sensor consisting of an array of PCFs is developed to differentiate various water/EtOH mixtures based on their wetting behaviour on the fabricated PCFs. The wetting time was fixed to be 10 sec for all of the experiments (see appendix C).

5.1. Effect of neck angle on wetting behaviour of PCFs

In this section, the effect of neck angle on the wetting behaviour of PCFs is studied. The amounts of PMMA and water used were 20 µL and 430 µL, respectively to achieve PCFs with 4 layers and all the PCFs were coated with 9FS. The amount of TEOS used in each PCF was increased from 1.1 µL in PCF 1 to 3 µL in PCF 6. Based on Fig. 5.1, increasing the amount of TEOS results in decrease in neck angle from 32° ± 2° to 20° ± 2°. When the sample was immersed in W25, all PCFs were remained non-wetted since the contact angle of W25 (θ_C = 34° ± 1°) is greater than neck angles of all 6 PCFs ($\theta_C > \varphi_0$ is required for wetting). When the sample was immersed in W10, all PCFs were wetted since their neck angles are greater than contact angle of W10 (θ_C = 19° ± 1°). By changing the amount of TEOS, it is possible to control the values of neck angles in the PCFs and hence the wettability of the PCFs.

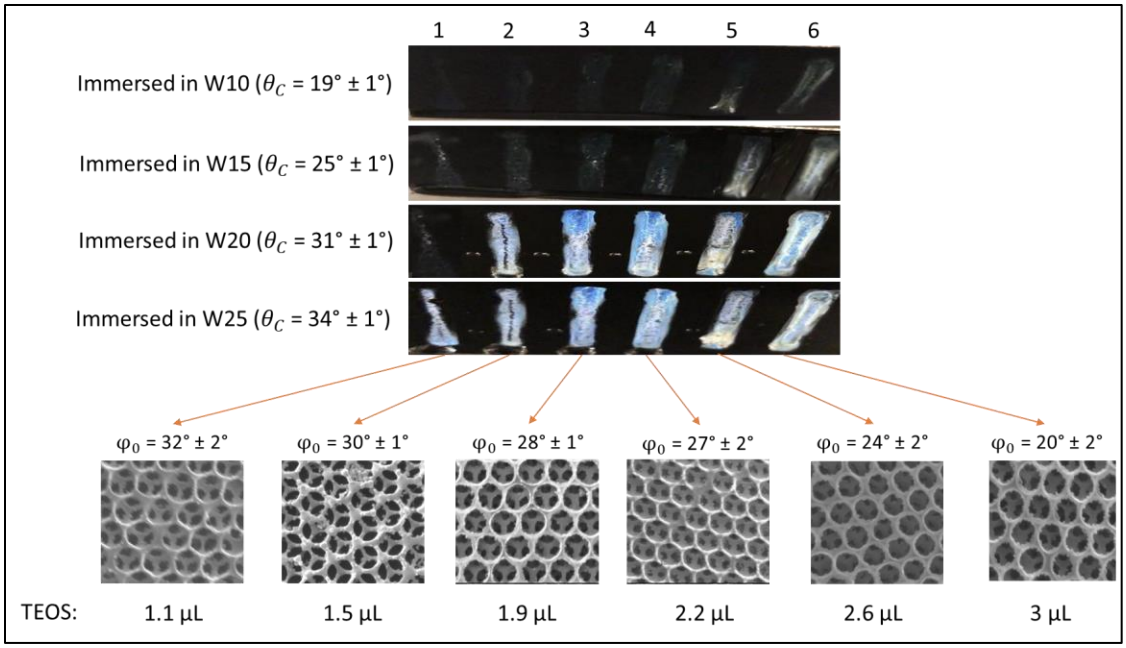

Figure 5.1. Effect of neck angle on the wettability of PCFs. In the image of the silicon strip, PCFs 1-6 are arranged from left to right. These PCFs were coated with 9FS.

5.2. Effect of chemical coatings on wetting behaviour of PCFs

In this section, the effect of chemical coating on wetting behaviour of PCFs is investigated. The amounts of PMMA, TEOS and water used in the template/matrix mixture were 24 µL, 1.7 µL and 700 µL, respectively, to achieve PCFs with 3 layers. All six PCFs have the same composition and thickness. Fig. 5.2 represents the effect of chemical coatings (i.e. TPMA, TMS, 3FS and 9FS) on wetting behaviour of an array of PCFs, with the uncoated PCFs as the control. All water/EtOH mixtures shown in Fig. 5.2 wetted the uncoated sample. The TPMA-coated sample remained not-wetted when it was immersed in W80 and W85; but it was wetted when immersed in W75 or the mixtures of higher EtOH contents. The higher the water content in the water/EtOH mixtures is, the higher is the contact angle of the mixtures, and it is harder for them to wet the PCFs. The wetting threshold for a TPMA-coated sample can be indicated as between W75 and W80 (i.e. W75-W80). As a result of a higher hydrophobicity of the TMS-coated sample, the wetting threshold was shifted to mixtures with lower EtOH contents, i.e. (W60-W65). When the samples were coated with 3FS and 9FS with greater hydrophobicities, the wetting

thresholds were further shifted to W40-W45 and W15-W20, respectively. Therefore, by using different chemical coatings, the wettability of the PCFs can be tuned.

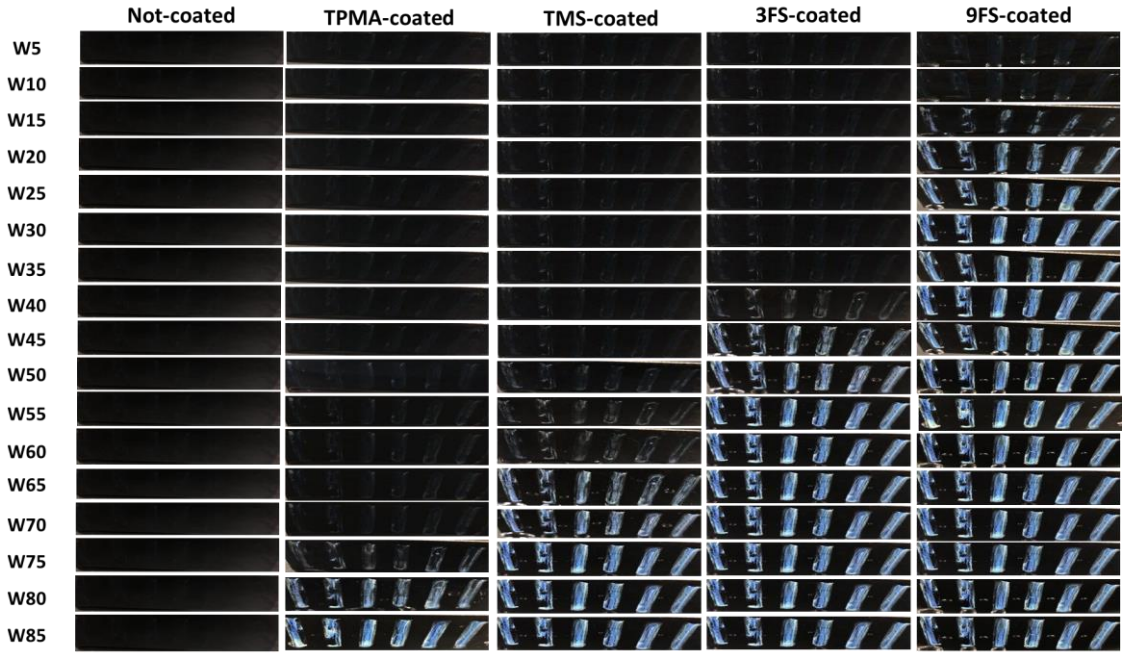

Figure 5.2. Effect of chemical coatings on the wetting behaviour of an array of PCFs coated with TPMA, TMS, 3FS and 9FS. All six PCFs have the same composition and thickness.

5.3. Effect of thickness on wetting behaviour of PCFs

In this section, the effect of thickness (in terms of number of layers) on wetting behaviour of PCFs is investigated. Two PCFs were fabricated using PMMA, TEOS and water amounts of 45 µL, 2.8 µL and 1300 µL (for 3 layers) and 50 µL, 3.1 µL and 510 µL (for 8 layers), respectively. The determinations of 3 and 8 layers were shown in Appendix D. Both samples were coated with 9FS. Since the TEOS/PMMA ratio for both samples was fixed to 0.062, we expect the PCFs should have the same neck angle and have the same wetting threshold. However, Fig. 5.3 shows the difference of thickness on wetting behaviour of PCFs with 3 and 8 layers. Based on Fig. 5.3, when the 3-layers sample was immersed in W15, all PCFs were wetted. On the other hand, when the 8-layers sample was immersed in W15, all PCFs were remained not-wetted. Therefore, the thickness is another factor that can be used to tune the wettability of PCFs.

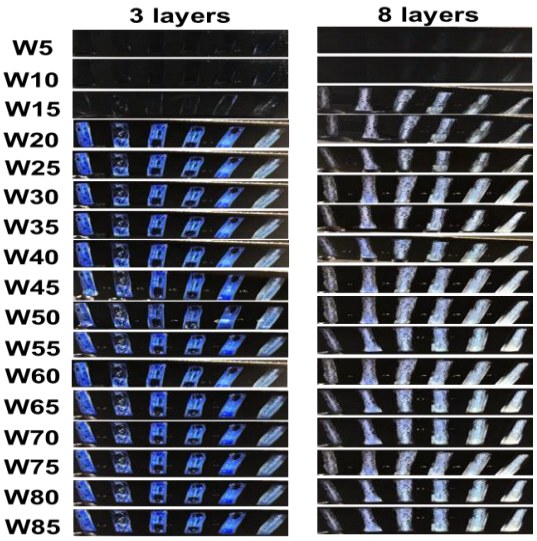

Figure 5.3. Effect of thickness on wetting behaviour of PCFs with 3 and 8 layers. All six PCFs in each silicon strip have the same composition. These PCFs were coated with 9FS.

5.4. Combinations of neck angle, thickness and chemical coating to tune wettability

In this section, combinations of neck angle, thickness and chemical coating are used to tune wettability of PCFs for differentiation of various water/EtOH mixtures.

To understand the combination of the three factors in a systematic way, we defined the excess ratio over theoretically required amount of TEOS (EXR) as a quantity that can be calculated based on the actual amount of TEOS used to fabricate a PCF. For example, for a PCF with the amount of PMMA, TEOS and water of 45, 2.8 and 1300 µL respectively, the theoretical amount of TEOS to fill 26% of the volume of the PCF is 1.4 µL. However, the actual amount of TEOS used to fabricate the PCF was 2.8 µL (note: different number of layers can have different theoretical values. For example, the theoretical values based on a computer algorithm[70] for 2, 3 and 5 layers have been found to be 32%, 30% and 28% respectively. In the present study 26% was used as a reference point to calculate EXR values for all the samples). Then by dividing 2.8 µL (actual amount used) over 1.4 µL (theoretical amount needed), the EXR is calculated to be 2. The greater the value of EXR is, the thicker is the walls of the PCF, the lower is the value of the neck angle and the lower is the tendency of pore wetting.

Table 5.1 shows the details for the compositions of the samples that are produced in this section. Five samples with different thicknesses and EXR values are produced.

Table 5.1. Composition of six PCFs on a silicon strip with thickness of 2, 3, 4, 6 and 8 layers. The six PCFs are PCFs 1-6 arranged from left to right in the images of the silicon strip. As described in Section 2.4, TEOS is composed of 0.01 M HCl/TEOS/EtOH in wt ratio of 1:1:1.5, and PMMA consists of 1% solid content

Thickness	Composition	PCF 1	PCF 2	PCF 3	PCF 4	PCF 5	PCF 6
A: 2 layers	PMMA	17 µL	17 µL	17 µL	17 µL	17 µL	17 µL
	TEOS	1.4 µL	1.7 µL	2.1 µL	2.5 µL	2.8 µL	3.2 µL
	Water	750 µL	750 µL	750 µL	750 µL	750 µL	750 µL
	EXR	2.7	3.3	4	4.8	5.4	6.1
B: 3 layers	PMMA	18 µL	18 µL	18 µL	18 µL	18 µL	18 µL
	TEOS	1.1 µL	1.5 µL	1.9 µL	2.2 µL	2.6 µL	3 µL
	Water	520 µL	520 µL	520 µL	520 µL	520 µL	520 µL
	EXR	2	2.7	3.4	4	4.7	5.4
C: 4 layers	PMMA	20 µL	20 µL	20 µL	20 µL	20 µL	20 µL
	TEOS	0.9 µL	1.3 µL	1.7 µL	2 µL	2.3 µL	2.6 µL
	Water	430 µL	430 µL	430 µL	430 µL	430 µL	430 µL
	EXR	1.5	2.1	2.8	3.3	3.7	4.2
D: 6 layers	PMMA	25 µL	25 µL	25 µL	25 µL	25 µL	25 µL
	TEOS	0.6 µL	0.9 µL	1.2 µL	1.5 µL	1.8 µL	2.1 µL
	Water	350 µL	350 µL	350 µL	350 µL	350 µL	350 µL
	EXR	0.8	1.2	1.6	2	2.3	2.7
E: 8 layers	PMMA	25 µL	25 µL	25 µL	25 µL	25 µL	25 µL
	TEOS	0.4 µL	0.7 µL	1 µL	1.3 µL	1.6 µL	1.8 µL
	Water	257 µL	257 µL	257 µL	257 µL	257 µL	257 µL
	EXR	0.5	0.9	1.3	1.7	2.1	2.3

Fig. 5.4 shows the wetting results of TPMA-coated samples after immersing in various water/EtOH mixtures. In each sample, the value of EXR increases from PCF 1 to PCF 6 (left to right). The different numbers of layers add another quantifier to these PCFs; for instance, for PCFs with 6 layers, they are called PCFs D1-6, and for 8 layers, they are called PCFs E1-6. Based on Fig. 5.4 in order to differentiate between W60 and W70, TPMA-coated samples with 6 or 8 layers can be used. In the case of 8 layers, W65 wetted PCF E1 only, but W60 wetted all PCFs E1-6. In the case of 6 layers, W65 wetted PCFs D1-4, but W60 wetted all PCFs D1-6.

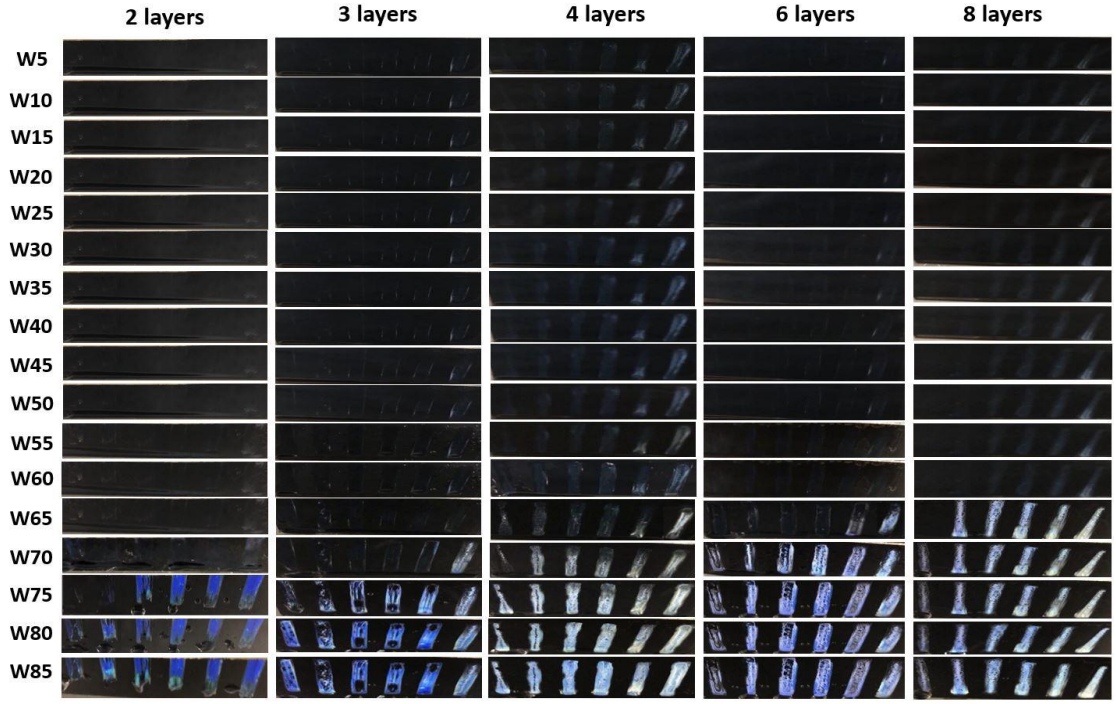

Figure 5.4. Effect of thickness on the wettability of PCFs when coated with TPMA.

Fig. 5.5 shows the wetting results of TMS-coated samples after immersing in various water/EtOH mixtures. Based on Fig. 5.5, in order to differentiate between W60 and W50, TMS-coated samples with 3, 4 and 6 layers can be used. Also, to differentiate between W50 and W40, TMS-coated samples with 8 layers can be used.

Fig 5.6 shows the wetting results of 3FS-coated samples after immersing in various water/EtOH mixtures. Based on Fig. 5.6, in order to differentiate W40 and W30, 3FS-coated samples with 3, 4, 6 and layers can be used.

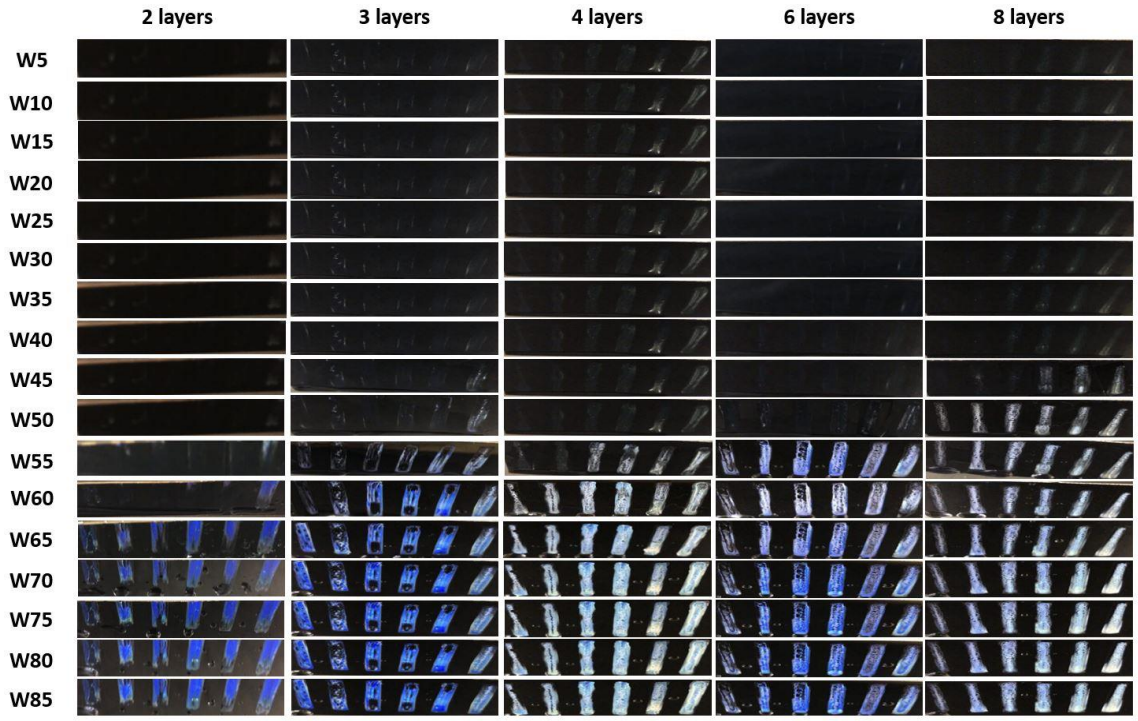

Figure 5.5. Effect of thickness on the wettability of PCFs when coated with TMS.

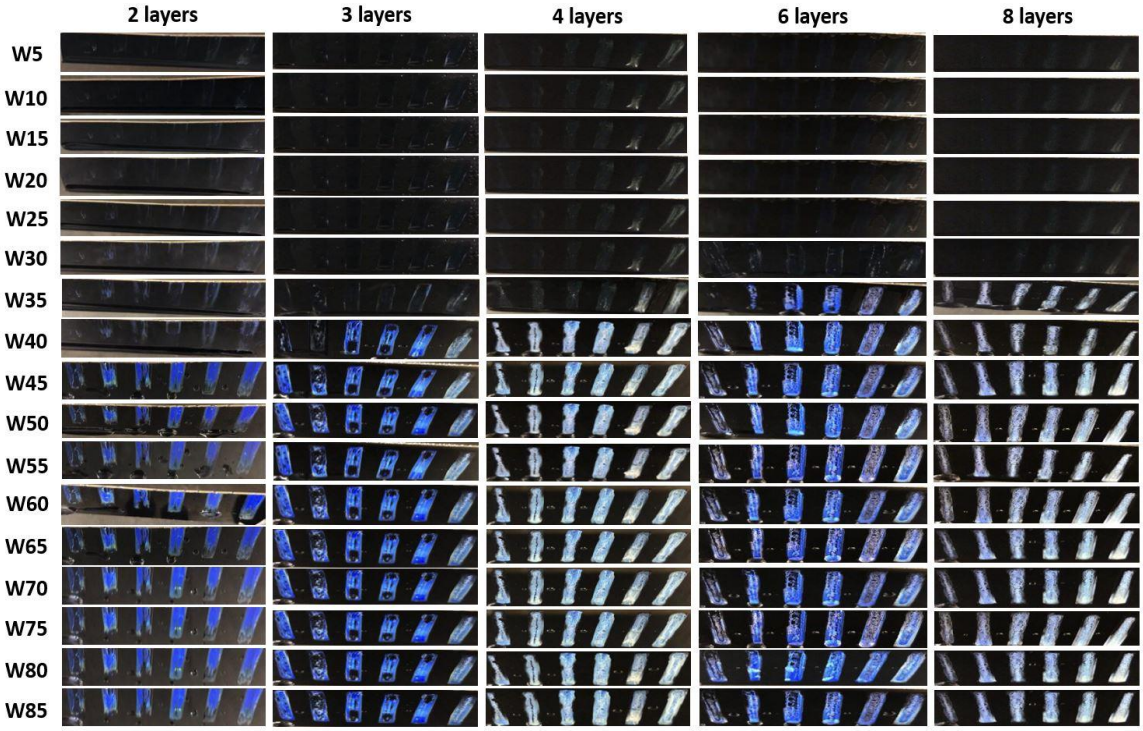

Figure 5.6. Effect of thickness on the wettability of PCFs when coated with 3FS

Fig. 5.7 shows the wetting results 9FS-coated samples after immersing in various water/EtOH mixtures. Based on Fig. 5.7, in order to differentiate between W25 and W20,

9FS-coated samples with 2 layers can be used. Also, to differentiate between W20 and W10, 9FS-coated samples with 4, 6 and 8 layers can be used.

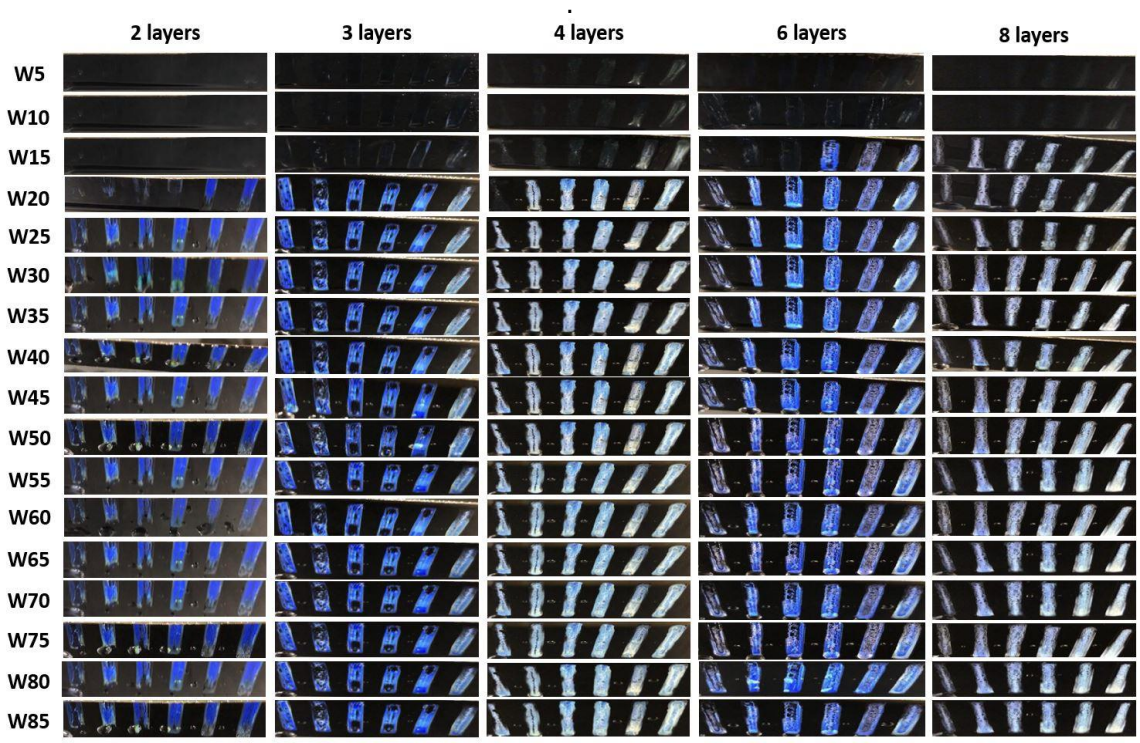

Figure 5.7. Effect of thickness on the wettability of PCFs when coated with 9FS.

Fig. 5.8 shows the plot of wetting threshold based on EXR and number of layers for the mixtures of W75, W70 and W65. These EXRs and layer values were extracted from Fig. 5.4. Based on Fig. 5.4, when a 2-layer TPMA-coated PCF is used, W75 wetted PCF B2 but not PCF B3. The wetting threshold EXR value was obtained by calculating the average of EXR value for PCF B2 (3.3) and for PCF B3 (4), which resulted in 3.7. Similarly, when a 3-layer TPMA-coated PCF was used, W75 wetted PCF C1 but not PCF C2. The wetting threshold was given by the average of EXR values for PCF C1 (2) and for PCF C2 (2.7), which resulted in 2.4. These two wetting thresholds for W75, i.e. (EXR=3.7, 2 layers) and (EXR=2.4, 3 layers), were then plotted in Fig. 5.8, and the two data points were joined to give the wetting threshold line in blue on the left.

The same procedure was followed to find other average EXR values and number of layers for the wetting thresholds of two other mixtures, i.e. W70 and W65. The obtained plot, as shown in Fig. 5.8, shows the threshold line of wetting, in which the wetted regions are on the left sides with green points, whereas non-wetted regions are on the right sides.

The wetting thresholds for PCFs coated with TMS, 3FS and 9FS using different liquid mixtures are also extracted and plotted in Figs. 5.9, 5.10 and 5.11, respectively.

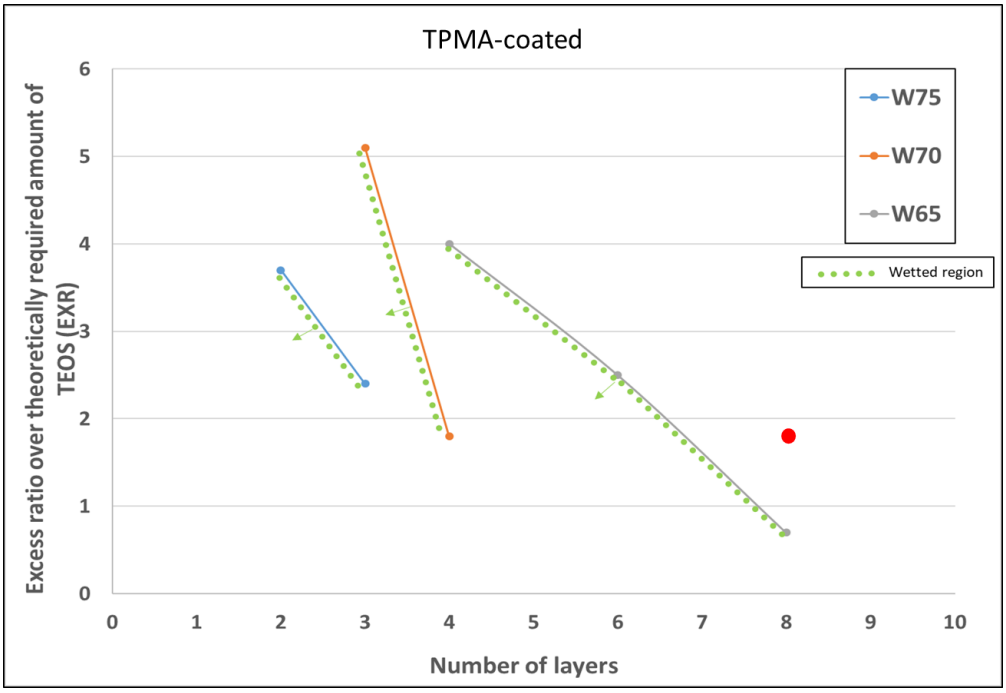

Figure 5.8. wetting threshold based on EXR and number of layers for TPMA-coated PCFs.

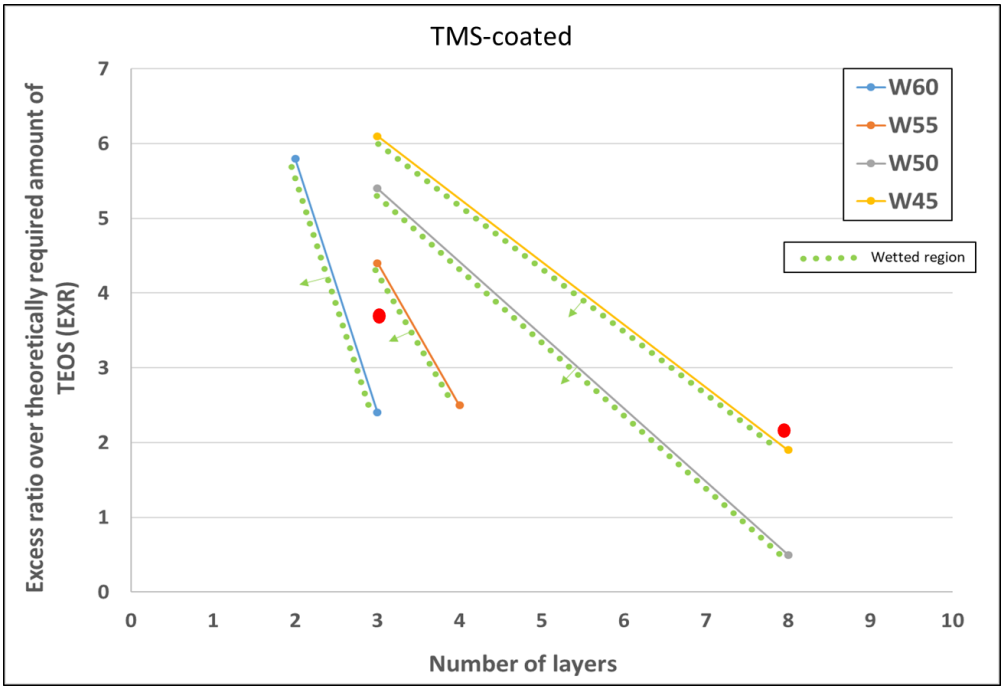

Figure 5.9. wetting threshold based on EXR and number of layers for TMS-coated PCFs.

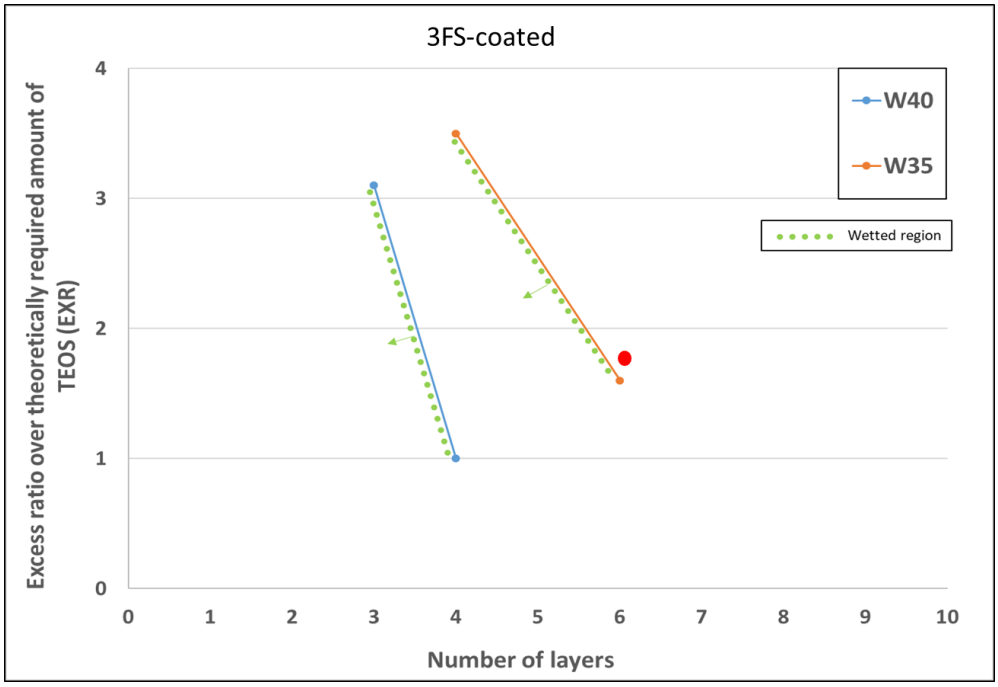

Figure 5.10. wetting threshold based on EXR and number of layers for 3FS-coated PCFs.

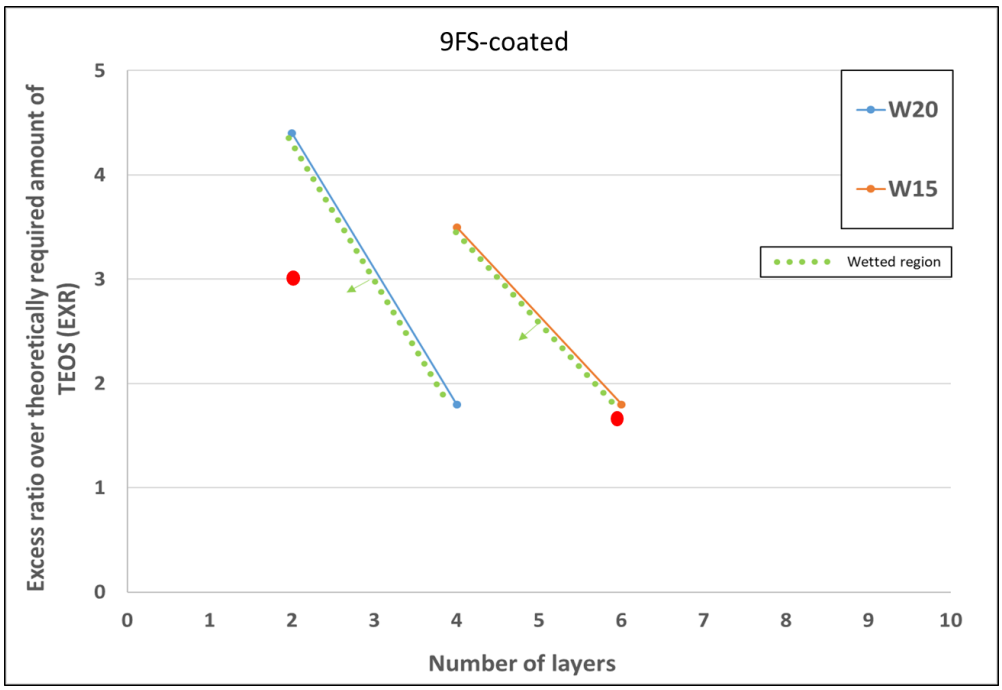

Figure 5.11. wetting threshold based on EXR and number of layers for 9FS-coated PCFs.

5.5. Development of a sensor to differentiate water/EtOH mixtures

Based on the wetting threshold graphs obtained in Section 5.4, a sensor strip platform was designed in order to differentiate between various water/EtOH mixtures. As it is shown in Fig 5.12, six different PCFs were produced with different chemical coatings, EXR and film thicknesses. In order to differentiate between W70 and W60, an 8-layer PCF was fabricated with EXR of 1.6 and with TPMA as chemical coating, see the red dot in Fig. 5.8. To differentiate between W60 and W50 a 3-layer PCF was fabricated with EXR of 3.6 and coating of TMS, and to differentiate between W50 and W40 an 8-layer PCF was fabricated with an EXR of 2.1 which was coated with TMS, see the two red dots in Fig. 5.9. In order to differentiate between W40 and W30, a 6-layer PCF was fabricated with an EXR of 1.6 which was coated with 3FS, see the red dot in Fig. 5.10. To differentiate between W30 and W20, a 2-layer PCF was made with an EXR and chemical coating of 3 and 9FS, respectively, and between W20 and W10, a 6-layer PCF was produced and coated with 9FS and the EXR was designed to be 1.8, see the two red dots in Fig. 5.11. The ideal image of differentiation is shown in Fig 5.12, in which the differentiation can be achieved by counting the number of wetted/not-wetted PCFs on the sensor strip.

Fig. 5.13 shows the image of the fabricated sensor and wetting results in W10, W20, W30, W40, W50, W60 and W70. Based on Fig. 5.13, the differentiation of 7 water/EtOH mixtures have been accomplished successfully. The final sensor strip shows 6 wetted PCFs when immersed in W10 (or a mixture with higher EtOH contents). If only one PCF is not wetted after immersion in a water/EtOH mixture, the mixture is considered to be W20. The final sensor shows 2, 3, 4, 5, and 6 non-wetted PCFs when immersed in W30, W40, W50, W60, and W70 (or a mixture with lower EtOH contents).

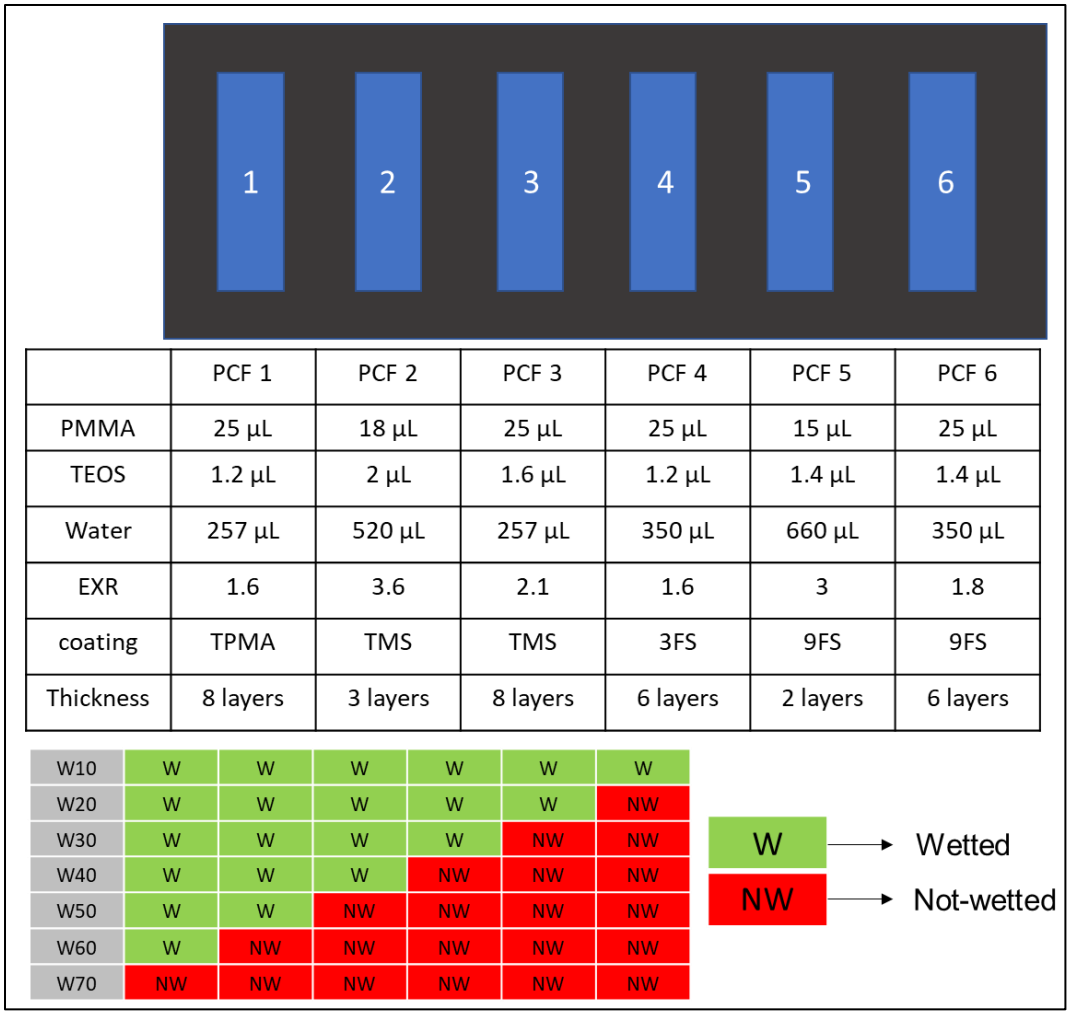

	PCF 1	PCF 2	PCF 3	PCF 4	PCF 5	PCF 6
PMMA	25 µL	18 µL	25 µL	25 µL	15 µL	25 µL
TEOS	1.2 µL	2 µL	1.6 µL	1.2 µL	1.4 µL	1.4 µL
Water	257 µL	520 µL	257 µL	350 µL	660 µL	350 µL
EXR	1.6	3.6	2.1	1.6	3	1.8
coating	TPMA	TMS	TMS	3FS	9FS	9FS
Thickness	8 layers	3 layers	8 layers	6 layers	2 layers	6 layers

W10	W	W	W	W	W	W
W20	W	W	W	W	W	NW
W30	W	W	W	W	NW	NW
W40	W	W	W	NW	NW	NW
W50	W	W	NW	NW	NW	NW
W60	W	NW	NW	NW	NW	NW
W70	NW	NW	NW	NW	NW	NW

W → Wetted

NW → Not-wetted

Figure 5.12. Schematic design and composition details of six PCFs on the sensor to differentiate seven different water/EtOH mixtures: W10, W20, W30, W40, W50, W60 and W70.

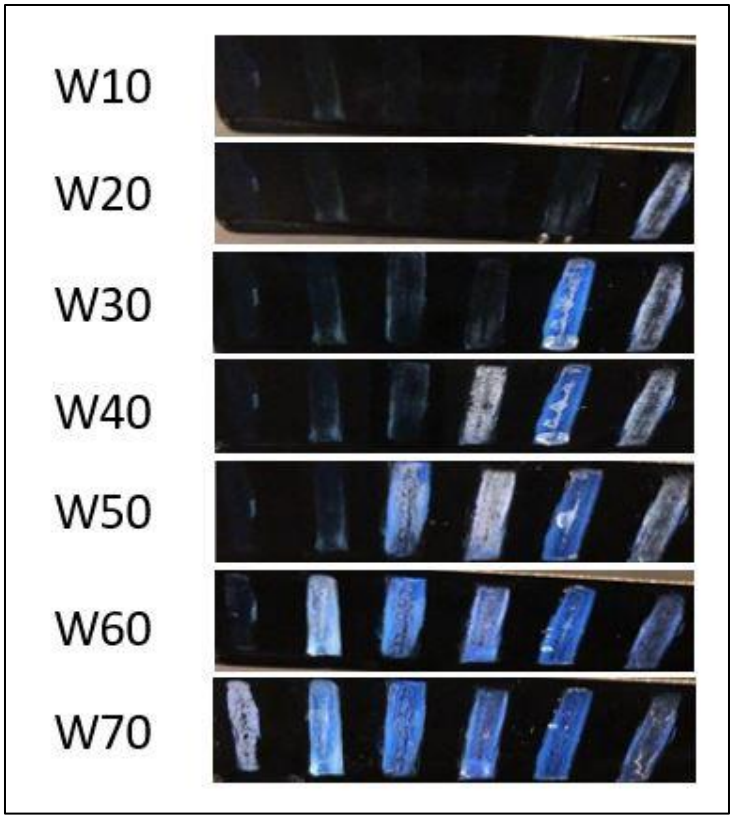

Figure 5.13. Differentiation of W10, W20, W30, W40, W50, W60 and W70 using an array of PCFs on a single sensor strip substrate.

The present work is compared with previously reported work. As shown in Table 5.2., the PCF preparation time, chemical coating, liquid mixtures for differentiation, and differentiation methods in previous reports and the present work are summarized. In this study, the PCF preparation time of 17 h was achieved which is much lower than the previously reported times (55 h). The final sensor in the present study can be used to differentiate a wider range of water/ethanol mixtures (W10 to W70) as compared to previous work. Moreover, the differentiation method in the present study is based on counting the number of wetted/non-wetted PCFs, which is more easily interpreted than the method of considering color pattern changes found in some of the previous reports.

Table 5.2. Summary of PCF preparation time, chemical coating, liquid mixtures for differentiation, and differentiation methods reported in literature.

<table>
<tr><th></th><th>A</th><th>B</th><th>C</th><th>D</th><th>E</th></tr>
<tr><td>PCF preparation time</td><td>55 h</td><td>55 h</td><td>55 h</td><td>NA</td><td>17 h</td></tr>
<tr><td>Chemical coating</td><td>13FS, DEC, 3FS, TMS</td><td>3FS, 13FS, DEC, 5FP, PTOL, TMS</td><td>13FS, DEC</td><td>p(DR1A-co-AA)</td><td>TPMA, TMS, 3FS, 9FS</td></tr>
<tr><td>Liquid mixtures for differentiation</td><td rowspan="2">(W0–W15–W22–W50)</td><td>(W10–W20)</td><td rowspan="2">(W0-W2.5-W5-W7.5)</td><td>(W90-W87.5)
(W90-W92.5)
(W92.5-W95)
(W95-W97.5)
(W97.5-W100)</td><td rowspan="2">(W10-W20-W30-W40-W50-W60-W70)</td></tr>
<tr><td>(W15-W25-W50)</td></tr>
<tr><td>Differentiation method</td><td>Wetted/non-wetted</td><td>Color patterns</td><td>Color patterns</td><td>Wetted/non-wetted</td><td>Wetted/non-wetted</td></tr>
<tr><td>References</td><td>58</td><td>60</td><td>61</td><td>62</td><td>Present work</td></tr>
</table>

3FS, 9FS, 13FS, 17FS, TMS, DEC, 5FP, PTOL are Trichloro(3,3,3-trifluoropropyl)-silane, nonafluorohexyltrichlorosilane, trichloro(1H,1H,2H,2H-perfluorooctyl)silane, heptadecafluoro(1,1,2,2-tetrahydrodecyl), trichloromethylsilane, n-decylsilyl, pentafluorophenylpropyl, p-tolyl, respectively.

Chapter 6.

Conclusions and future directions

6.1. Summary of the research and conclusion

In this study, an array of photonic crystal films (PCFs) was fabricated on a single substrate using co-assembly sedimentation. Factors such as template/matrix deposition method, sedimentation time, evaporation rate and TEOS/PMMA ratio which affect the quality of fabricated PCFs were studied. The optimum conditions for producing uniform PCFs with a bright structural color were obtained.

The fabricated PCFs were characterized using reflectance spectra, optical and SEM images and the origin of the blue structural color was verified. Experimental results showed a good agreement with theoretical calculations, which verified our observations.

Interfacial properties of various water/EtOH mixtures on 4 different chemical coatings of TPMA, TMS, 3FS and 9FS were investigated. Water/EtOH mixtures showed a decrease in contact angle when the EtOH content of the mixture was increased. TPMA, TMS, 3FS and 9FS showed an increasing trend in hydrophobicity.

The effects of chemical coating, neck angle and thickness on the PCF wettability were studied individually. A more hydrophobic chemical coating, a smaller neck angle and a larger film thickness, result in more difficult wetting of PCF pores.

Combinations of different chemical coatings, neck angles and film thicknesses were used to tune the wettability of the PCFs for various water/EtOH mixtures with 5% EtOH difference. Based on the optimized combinations of 3 factors, a final sensor strip platform was designed to differentiate between 7 water/EtOH mixtures.

The final developed sensor is capable of differentiating between 7 water/EtOH mixtures: W10, W20, W30, W40, W50, W60 and W70 by counting the number of wetted and not-wetted PCFs. The results of six, five, four, three, two, one and zero wetted PCFs after immersion in a water/EtOH mixtures can be attributed to W10 (or a mixture with a higher EtOH content), W20, W30, W40, W50, W60 and W70 (or a mixture with a lower EtOH content).

6.2. Future directions

In order to differentiate between water/EtOH mixtures with lower EtOH content new chemical coatings which show a lower hydrophobicity than TPMA must be used. By using less hydrophobic chemical coatings, differentiation of W80, W90 and W100 may also be achieved.

The use of lower ratios of TEOS/PMMA may produce bigger neck angles, which may in turn be used to differentiate water/EtOH mixtures with lower amounts of EtOH.

The production of an array of 12 or more PCFs on a single substrate may increase the multiplex advantage for differentiation of water/EtOH mixtures. The use of more PCFs on a substrate can be helpful to increase the resolution of the sensor from a difference of 10% to 5% EtOH in the water/EtOH mixture.

The same sensor strip platform should also be used to differentiate other liquid mixtures such as the mixtures of different alkanes. The mixtures should have sufficiently large difference in contact angles in order to be used in this platform.

References

(1) Von Freymann, G.; Kitaev, V.; Lotsch, B. V.; Ozin, G. A. Bottom-up Assembly of Photonic Crystals. *Chem. Soc. Rev.* **2013**, *42* (7), 2528–2554.

(2) Yablonovitch, E. Inhibited Spontaneous Emission in Solid-State Physics and Electronics. *Phys. Rev. Lett.* **1987**, *58* (20), 2059–2062.

(3) John, S. Strong Localization of Photons in Certain Disordered Dielectric Superlattices. *Phys. Rev. Lett.* **1987**, *58* (23), 2486–2489.

(4) Qihuang, G.; Hu, X. *Photonic Crystals: Principles and Applications*; Taylor & Francis Group CRC Press,: Boca Raton, FL, 2013.

(5) Sibilia, C.; Benson, T. M.; Marciniak, M.; Szoplik, T. *Photonic Crystals: Physics and Technology*; Springer: Verlag Mailand, 2008.

(6) Khaled, D. El; Castellano, N. N.; Gázquez, J. A.; Manzano-agugliaro, F. Dielectric Spectroscopy in Biomaterials : Agrophysics. **2016**, *9* (5), 310:1-26.

(7) Benisty, H.; Berger, V.; Gerard, J.-M.; Maystre, D.; Tchelokov, A. *Photonic Crystals: Towards Nanoscale Photonic Devices*; Springer: Verlag Berlin Heidelberg, 2008.

(8) Fenzl, C.; Hirsch, T.; Wolfbeis, O. S. Photonic Crystals for Chemical Sensing and Biosensing. *Angew. Chemie - Int. Ed.* **2014**, *53* (13), 3318–3335.

(9) Sharp, D. N.; Campbell, M.; Dedman, E. R.; Harrison, M. T.; Denning, R. G.; Turberfield, A. J. Photonic Crystals for the Visible Spectrum by Holographic Lithography. *Opt. Quantum Electron.* **2002**, *34* (3), 3–12.

(10) Jeon, S.; Park, J.-U.; Cirelli, R.; Yang, S.; Heitzman, C. E.; Braun, P. V.; Kenis, P. J. A.; Rogers, J. A. Fabricating Complex Three-Dimensional Nanostructures with High-Resolution Conformable Phase Masks. *Proc. Natl. Acad. Sci.* **2004**, *101* (34), 12428–12433.

(11) Zheng, H.; Ravaine, S. Bottom-Up Assembly and Applications of Photonic Materials. *Crystals* **2016**, *6* (5), 54:1-25.

(12) Kim, T. W. The Applications for 3D Inverse Opal Microstructures, University of Illinois at Urbana-Champaign, 2011.

(13) Li, F.; Josephson, D. P.; Stein, A. Colloidal Assembly: The Road from Particles to Colloidal Molecules and Crystals. *Angew. Chemie - Int. Ed.* **2011**, *50* (2), 360–388.

(14) Li, Q.; Jonas, U.; Zhao, X. S.; Kappl, M. The Forces at Work in Colloidal Self-

Assembly: A Review on Fundamental Interactions between Colloidal Particles. *Asia-Pac. J. Chem. Eng.* **2008**, *3*, 255–268.

(15) Walker, D. A.; Kowalczyk, B.; De La Cruz, M. O.; Grzybowski, B. A. Electrostatics at the Nanoscale. *Nanoscale* **2011**, *3* (4), 1316–1344.

(16) Kaplan, P. D.; Rouke, J. L.; Yodh, A. G.; Pine, D. J. Entropically Driven Surface Phase Separation in Binary Colloidal Mixtures. *Phys. Rev. Lett.* **1994**, *72* (4), 582–585.

(17) Liu, G.; Shao, J.; Zhang, Y.; Wu, Y.; Wang, C.; Fan, Q.; Zhou, L. Self-Assembly Behavior of Polystyrene/Methacrylic Acid (P(St-MAA)) Colloidal Microspheres on Polyester Fabrics by Gravitational Sedimentation. *J. Text. Inst.* **2015**, *106* (12), 1293–1305.

(18) Mastrangeli, M.; Abbasi, S.; Varel, C.; Van Hoof, C.; Celis, J. P.; Böhringer, K. F. Self-Assembly from Milli- to Nanoscales: Methods and Applications. *J. Micromech. Microeng.* **2009**, *19* (8), 083001.

(19) Zhang, J.; Sun, Z.; Yang, B. Self-Assembly of Photonic Crystals from Polymer Colloids. *Curr. Opin. Colloid Interface Sci.* **2009**, *14* (2), 103–114.

(20) Stein, A.; Li, F.; Denny, N. R. Morphological Control in Colloidal Crystal Templating of Inverse Opals, Hierarchical Structures and Shaped Particles. *Chem. Mater.* **2008**, *20* (3), 649–666.

(21) Mocanu, A.; Rusen, E.; Diacon, A. Optical Properties of the Self-Assembling Polymeric Colloidal Systems. *Int. J. Polym. Sci.* **2013**, *2013*, 238567:1-11.

(22) Ge, J.; Yin, Y. Responsive Photonic Crystals. *Angew. Chemie - Int. Ed.* **2011**, *50* (7), 1492–1522.

(23) Wang, H.; Zhang, K. Q. Photonic Crystal Structures with Tunable Structure Color as Colorimetric Sensors. *Sensors* **2013**, *13* (4), 4192–4213.

(24) Chabanov, A. A.; Jun, Y.; Norris, D. J. Avoiding Cracks in Self-Assembled Photonic Band-Gap Crystals. *Am. Inst. Phys.* **2004**, *84* (18), 3573–3575.

(25) Wong, S.; Kitaev, V.; Ozin, G. A. Colloidal Crystal Films: Advances in Universality and Perfection. *J. Am. Chem. Soc.* **2003**, *125* (50), 15589–15598.

(26) Hatton, B.; Mishchenko, L.; Davis, S.; Sandhage, K. H.; Aizenberg, J. Assembly of Large-Area, Highly Ordered, Crack-Free Inverse Opal Films. *Proc. Natl. Acad. Sci.* **2010**, *107* (23), 10354–10359.

(27) Ma, C.; Jiang, Y.; Yang, X.; Wang, C.; Li, H.; Dong, F.; Yang, B.; Yu, K.; Lin, Q. Centrifugation-Induced Water-Tunable Photonic Colloidal Crystals with Narrow Diffraction Bandwidth and Highly Sensitive Detection of SCN-. *ACS Appl. Mater.*

Interfaces **2013**, *5* (6), 1990–1996.

(28) Ko, Y. G.; Shin, D. H.; Lee, G. S.; Choi, U. S. Fabrication of Colloidal Crystals on Hydrophilic/Hydrophobic Surface by Spin-Coating. *Colloids Surf A Physicochem Eng Asp* **2011**, *385* (1–3), 188–194.

(29) Zhou, Z.; Zhao, X. S. Flow-Controlled Vertical Deposition Method for the Fabrication of Photonic Crystals. *Langmuir* **2004**, *20* (4), 1524–1526.

(30) Deleuze, C.; Sarrat, B.; Ehrenfeld, F.; Perquis, S.; Derail, C.; Billon, L. Photonic Properties of Hybrid Colloidal Crystals Fabricated by a Rapid Dip-Coating Process. *Phys. Chem. Chem. Phys.* **2011**, *13* (22), 10681–10689.

(31) He, L.; Hu, Y.; Kim, H.; Ge, J.; Kwon, S.; Yin, Y. Magnetic Assembly of Nonmagnetic Particles into Photonic Crystal Structures. *Nano Lett.* **2010**, *10* (11), 4708–4714.

(32) Xu, X.; Friedman, G.; Humfeld, K. D.; Majetich, S. A.; Asher, S. A. Superparamagnetic Photonic Crystals. *Adv. Mater.* **2001**, *13* (22), 1681–1684.

(33) Reculusa, S.; Ravaine, S. Synthesis of Colloidal Crystals of Controllable Thickness through the Langmuir-Blodgett Technique. *Chem. Mater.* **2003**, *15* (2), 598–605.

(34) Holgado, M.; García-Santamaría, F.; Blanco, A.; Ibisate, M.; Cintas, A.; Míguez, H.; Serna, C. J.; Molpeceres, C.; Requena, J.; Mifsud, A.; et al. Electrophoretic Deposition to Control Artificial Opal Growth. *Langmuir* **1999**, *15* (14), 4701–4704.

(35) Reese, C. E.; Guerrero, C. D.; Weissman, J. M.; Lee, K.; Asher, S. A. Synthesis of Highly Charged, Monodisperse Polystyrene Colloidal Particles for the Fabrication of Photonic Crystals. *J. Colloid Interface Sci.* **2000**, *232* (1), 76–80.

(36) Ishikawa, K.; Harada, H.; Okubo, T. Formation Process of Three-Dimensional Arrays from Silica Spheres. *AIChE J.* **2003**, *49* (5), 1293–1299.

(37) Lewis, J. A. Colloidal Processing of Ceramics. *J. Am. Ceram. Soc.* **2000**, *83* (10), 2341–2359.

(38) Liau, L. C.; Huang, Y. Process Optimization of Sedimentation Self-Assembly of Opal Photonic Crystals under Relative Humidity-Controlled Environments. *Expert Syst. Appl.* **2008**, *35* (3), 887–893.

(39) Kuai, S. L.; Hu, X. F.; Haché, A.; Truong, V. V. High-Quality Colloidal Photonic Crystals Obtained by Optimizing Growth Parameters in a Vertical Deposition Technique. *J. Cryst. Growth* **2004**, *267* (1–2), 317–324.

(40) McLachlan, M. A.; Johnson, N. P.; De La Rue, R. M.; McComb, D. W. Thin Film Photonic Crystals: Synthesis and Characterisation. *J. Mater. Chem.* **2004**, *14* (2),

144–150.

(41) Liu, G. Q.; Wang, Z. S.; Ji, Y. H. Influence of Growth Parameters on the Fabrication of High-Quality Colloidal Crystals via a Controlled Evaporation Self-Assembly Method. *Thin Solid Films* **2010**, *518* (18), 5083–5090.

(42) Zhou, L.; Wu, Y.; Liu, G.; Li, Y.; Fan, Q.; Shao, J. Fabrication of High-Quality Silica Photonic Crystals on Polyester Fabrics by Gravitational Sedimentation Self-Assembly. *Color. Technol.* **2015**, *131* (6), 413–423.

(43) Ko, Y. G.; Shin, D. H. Effects of Liquid Bridge between Colloidal Spheres and Evaporation Temperature on Fabrication of Colloidal Multilayers. *J. Phys. Chem. B* **2007**, *111* (7), 1545–1551.

(44) Liau, L. C. K.; Huang, Y. K. Effects of Influential Factors on Sedimentation Self-Assembly Processing of Photonic Band Gap Crystals by Relative Humidity-Controlled Environments. *Chem. Eng. Process. Process Intensif.* **2008**, *47* (9–10), 1578–1584.

(45) Dimitrov, A. S.; Nagayama, K. Continuous Convective Assembling of Fine Particles into Two-Dimensional Arrays on Solid Surfaces. *Langmuir* **1996**, *12* (5), 1303–1311.

(46) Li, Z.; Wang, J.; Song, Y. Particuology Self-Assembly of Latex Particles for Colloidal Crystals. *Particuology* **2011**, *9* (6), 559–565.

(47) Parola, A.; Buzzaccaro, S.; Secchi, E.; Piazza, R. Sedimentation Equilibrium and the Generalized Archimedes' Principle. *J. Chem. Phys.* **2013**, *138* (11), 114907.

(48) Verhoeff, A. A.; Van Rijssel, J.; De Villeneuve, V. W. A.; Lekkerkerker, H. N. W. Orientation Dependent Stokes Drag in a Colloidal Liquid Crystal. *Soft Matter* **2008**, *4* (8), 1602–1604.

(49) William E. Boyce, R. C. D. *Elementary Differential Equations*; Wiley: New york, 2012.

(50) Burgess, I. B.; Lončar, M.; Aizenberg, J. Structural Colour in Colourimetric Sensors and Indicators. *J. Mater. Chem. C* **2013**, *1* (38), 6075–6086.

(51) Kinoshita, S.; Yoshioka, S. Structural Colors in Nature: The Role of Regularity and Irregularity in the Structure. *ChemPhysChem* **2005**, *6* (8), 1443–1459.

(52) Vogel, N.; Utech, S.; England, G. T.; Shirman, T.; Phillips, K. R.; Koay, N.; Burgess, I. B.; Kolle, M.; Weitz, D. A.; Aizenberg, J. Color from Hierarchy: Diverse Optical Properties of Micron-Sized Spherical Colloidal Assemblies. *Proc. Natl. Acad. Sci.* **2015**, *112* (35), 10845–10850.

(53) Tanaka, T.; Lee, J.; Scheller, P. R. Interfacial Free Energy and Wettability.

Treatise Process Metall. **2014**, *2*, 61–77.

(54) Wong, T. S.; Sun, T.; Feng, L.; Aizenberg, J. Interfacial Materials with Special Wettability. *MRS Bull.* **2013**, *38* (5), 366–371.

(55) Vogel, N.; Belisle, R. A.; Hatton, B.; Wong, T. S.; Aizenberg, J. Transparency and Damage Tolerance of Patternable Omniphobic Lubricated Surfaces Based on Inverse Colloidal Monolayers. *Nat. Commun.* **2013**, *4*, 2176:1-10.

(56) Phillips, K. R.; Vogel, N.; Burgess, I. B.; Perry, C. C.; Aizenberg, J. Directional Wetting in Anisotropic Inverse Opals. *Langmuir* **2014**, *30* (25), 7615–7620.

(57) Sedighi, A.; Qiu, S.; Wong, M. C. K.; Li, P. C. H. Dip-in Indicators for Visual Differentiation of Fuel Mixtures Based on Wettability of Fluoroalkylchlorosilane-Coated Inverse Opal Films. *ACS Appl. Mater. Interfaces* **2015**, *7* (51), 12387–12392.

(58) Burgess, I. B.; Mishchenko, L.; Hatton, B. D.; Kolle, M.; Lončar, M.; Aizenberg, J. Encoding Complex Wettability Patterns in Chemically Functionalized 3D Photonic Crystals. *J. Am. Chem. Soc.* **2011**, *133* (32), 12430–12432.

(59) Burgess, I. B.; Nerger, B. A.; Raymond, K. P.; Goulet-Hanssens, A.; Singleton, T. A.; Kinney, M. H.; Shneidman, A. V; Koay, N.; Barrett, C. J.; Lončar, M.; et al. Wetting in Color: From Photonic Fingerprinting of Liquids to Optical Control of Liquid Percolation. *Proc. SPIE - Int. Soc. Opt. Eng.* **2013**, *8632*, 863201.

(60) Raymond, K. P.; Burgess, I. B.; Kinney, M. H.; Lončar, M.; Aizenberg, J. Combinatorial Wetting in Colour: An Optofluidic Nose. *Lab Chip* **2012**, *12* (19), 3666–3669.

(61) Burgess, I. B.; Koay, N.; Raymond, K. P.; Kolle, M.; Lon, M.; Al, B. E. T. Wetting in Color : Colorimetric Differentiation of Organic Liquids with High Selectivity. *ACS Nano* **2012**, *6* (2), 1427–1437.

(62) Singleton, T. A.; Burgess, I. B.; Nerger, B. A.; Goulet-Hanssens, A.; Koay, N.; Barrett, C. J.; Aizenberg, J. Photo-Tuning of Highly Selective Wetting in Inverse Opals. *Soft Matter* **2014**, *10* (9), 1325–1328.

(63) Fujii, T. PDMS-Based Microfluidic Devices for Biomedical Applications. *Microelectron. Eng.* **2002**, *61*, 907–914.

(64) Marzancola, M. G. A Microfluidic Antibody Bioarray for Detection of Human Interleukins, Simon Fraser University, 2016.

(65) Zuhailawati, H.; Samayamutthirian, P.; Haizu, C. H. M.; Campus, E.; Pinang, P. Fabrication of Low Cost Aluminium Matrix Composite Reinforced with Silica Sand. *J. Phys. Sci.* **2007**, *18* (1), 47–55.

(66) Kim, D. Surface Modification of Indium Tin Oxide, Simon Fraser University, 2017.

(67) Goldstein, J. I.; Newbury, D. E.; Michael, J. R.; Ritchie, N. W. M.; Scott, J. H. J.; Joy, D. C. *Microscopy and X-Ray Microanalysis*; Springer: New York, NY, 2018.

(68) Khlebtsov, B. N.; Khanadeev, V. A.; Khlebtsov, N. G.; V, P. E.; Sarato, V.; State, S. V; Uni, V.; Astrakhanskaya, U.; Sarato, V. Determination of the Size , Concentration , and Refractive Index of Silica Nanoparticles from Turbidity Spectra. *Langmuir* **2008**, *24* (16), 8964–8970.

(69) Tao, C.; Yan, H.; Yuan, X.; Yin, Q.; Zhu, J.; Ni, W.; Yan, L.; Zhang, L. Colloids and Surfaces A : Physicochemical and Engineering Aspects Sol-Gel Based Antireflective Coatings with Superhydrophobicity and Exceptionally Low Refractive Indices Built from Trimethylsilanized Hollow Silica Nanoparticles. *Colloids Surfaces A Physicochem. Eng. Asp.* **2016**, *509*, 307–313.

(70) Private Communication from Ali Khajezade (Xajezade@mail.Ubc.ca) on March 18, 2019).

(71) Sirdeshmukh, D. B.; Sirdeshmukh, L.; Subhadra, K. G. *Crystallography. In: Atomistic Properties of Solids*; Springer Series in Materials Science: Berlin, 2011.

Appendix A.

Measurement of contact angles of various gasoline/oil mixtures on PCFs coated with 3FS and 9FS

Table A.1 shows the contact angles values obtained for different gasoline/oil mixtures on flat silicon substrates coated with 3FS and 9FS. Fig. A.1 shows the graph of these contact angles versus composition of liquids for different gasoline/oil mixtures. The difference in contact angles for the six gasoline/oil mixture was 5 degrees, which was insufficient for differentiation by PCFs using a single chemical coating. Other factors, such as neck angle and number of layers, should be considered for successful liquid composition differentiation.

Table A.1. Contact angles values obtained for different gasoline/oil mixtures on flat silicon substrates coated with 3FS and 9FS. SD represents the standard deviations for three measurements.

Gasoline/oil mixture	3FS	SD	9FS	SD
Oil	43.9	1.5	61.1	0.7
16:1	16.7	0.9	34.3	1.7
20:1	15.7	1.5	34.2	0.8
25:1	13.5	0.5	33.4	1.5
32:1	15.1	1.1	29.7	0.6
40:1	15.0	0.6	31.0	1.8
50:1	14.8	1.0	32.7	0.7
Gasoline	8.1	1.6	31.2	0.9

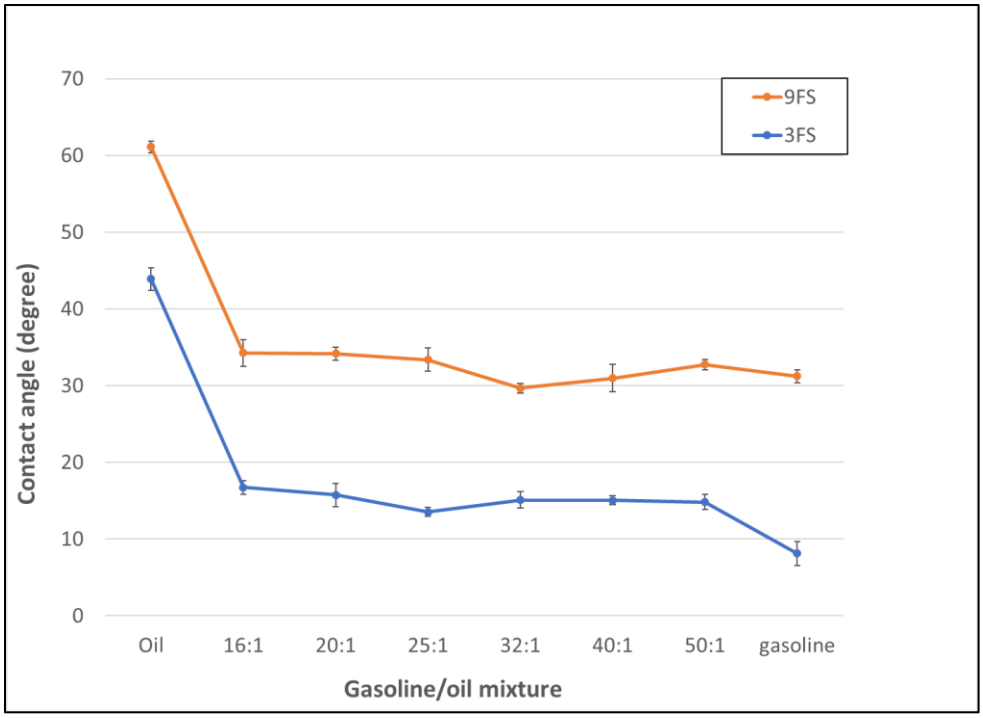

Figure A.1. **Graph of contact angles vs. composition of liquids for different gasoline/oil mixtures on silicon substrate coated with: nonafluorohexyltrichlorosilane (9FS) and trichloro (3,3,3-trifluoropropyl)-silane (3FS).**

Appendix B.

Change of measured contact angles with time

Fig. B.1 shows images of droplets of ethanol, water and different gasoline/oil mixtures on two coated silicon substrates captured after different intervals of time. Fig. B.2 shows the graph of contact angles versus time after liquid dispensing for water, oil, gasoline and 5 different gasoline/oil mixtures. Based on Fig. B.1 and Fig. B.2, the contact angles of volatile mixtures decrease over time, probably due to a change in the shape of droplets.

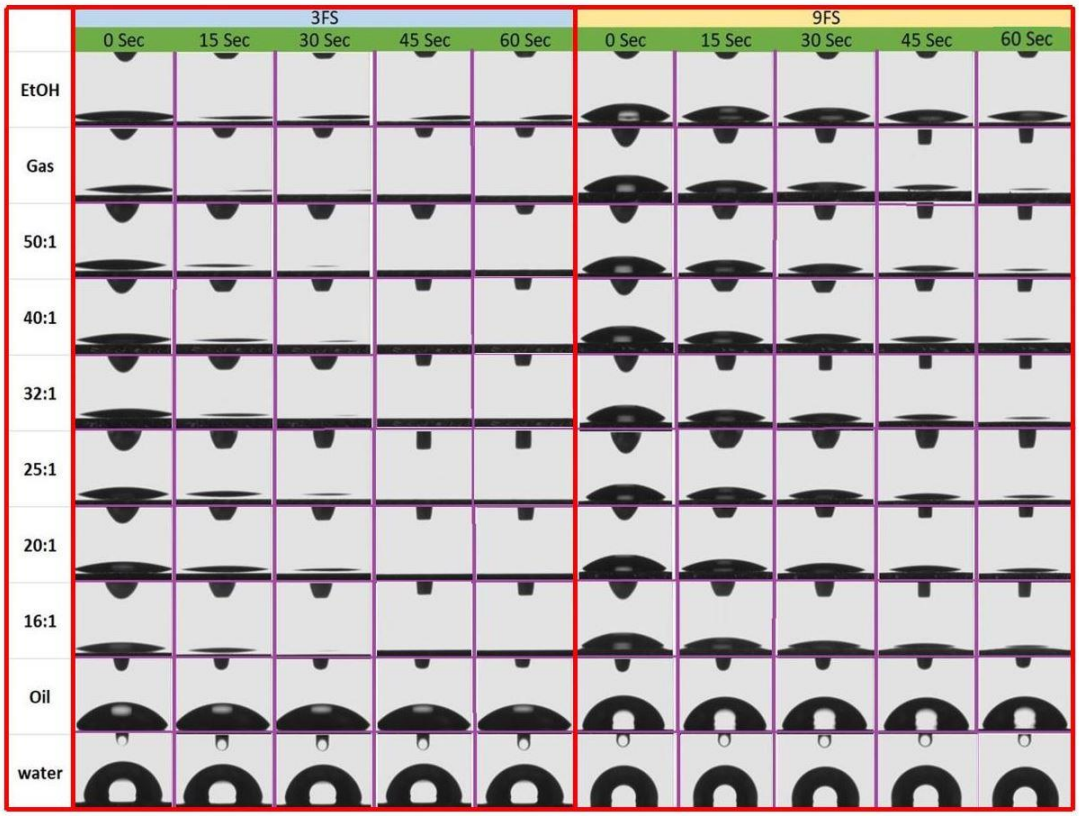

Figure B.1. Images of droplets of ethanol, water and different gasoline/oil mixtures on two coated silicon substrates captured after different intervals of time.

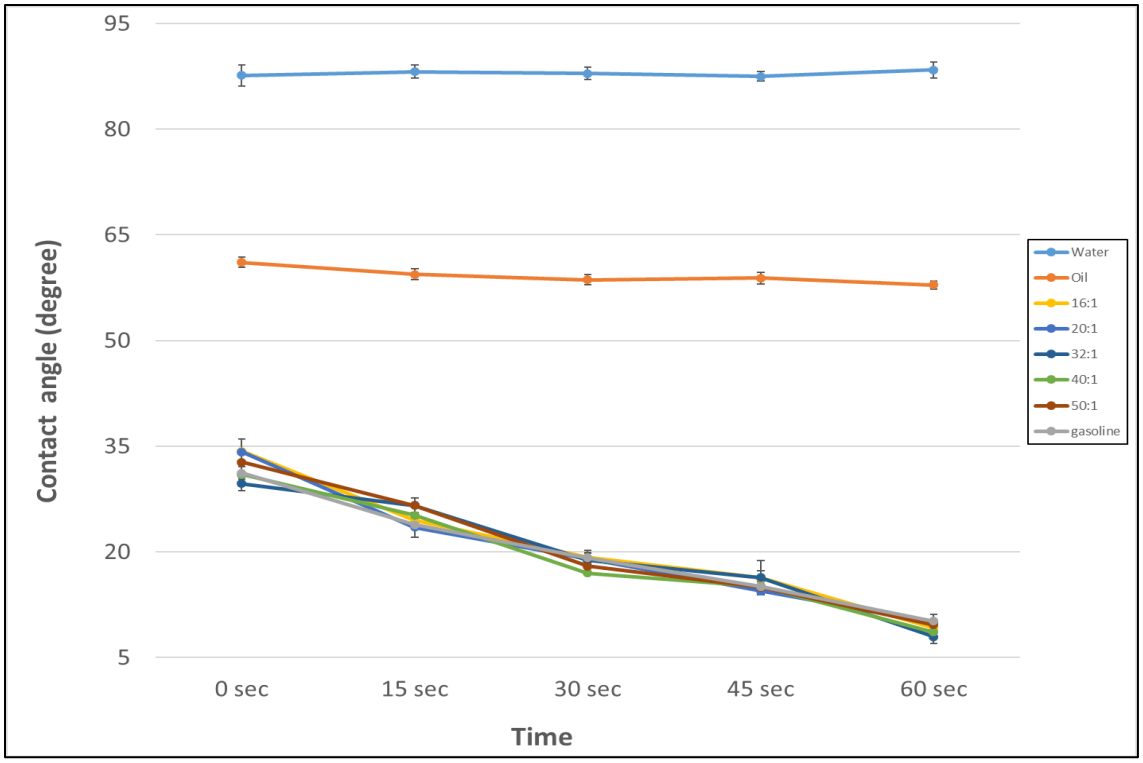

Figure B.2. Graph of contact angles vs. time after liquid dispensing for water, oil, gasoline and 5 different gasoline/oil mixtures.

Appendix C.

Time of liquid wetting experiments

Fig. C.1 shows the wetting behaviour of five PCFs over time when immersed in EtOH and water. The amounts of PMMA, TEOS and water used were 40 µL, 2.5 µL and 860 µL, respectively, to achieve 4 layers for all five PCFs. Based on Fig. C.1, the wetting behaviour of samples are similar for water or EtOH during different intervals of time. So, we fixed the wetting time to be 10 seconds in all subsequent experiments.

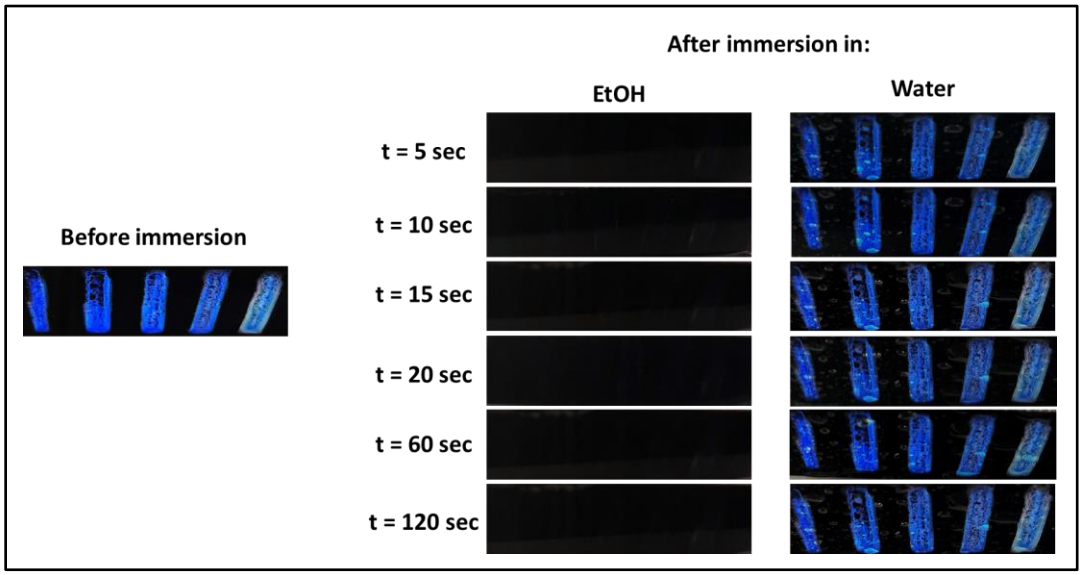

Figure C.1. Wetting behaviour of five PCFs over time when immersed in EtOH and water. The amouns of PMMA, TEOS and water used were 40, 2.5 and 860 µL, respectively to achieve 4 layers in all five PCFs.

Appendix D.

Determination of the number of layers

In order to estimate the number of layers of a PCF based on the amount of PMMA used, one must divide the number of PMMA particles used to the number of PMMA particles required to cover a complete monolayer. To calculate the number of particles required to attain one complete layer of PCF in each trench, the total area of the trench should be divided by the cross-section area occupied by each particle. In order to obtain a more accurate estimation of the required number of PMMA particles to cover a monolayer, the calculation was based upon an average number of pores in a top-view SEM image taken during this study (see Fig. D.1). Based on Fig. D.1, each set of 24 particles (19 full particles and 10 partial particles) occupied an area of 2.187×10^{-6} mm^2 (1444 nm × 1515 nm). The area of each trench (2.5 mm width – 20 mm length) was 50 mm^2. As a result, to form one complete layer, 5.49×10^8 PMMA particles were required.

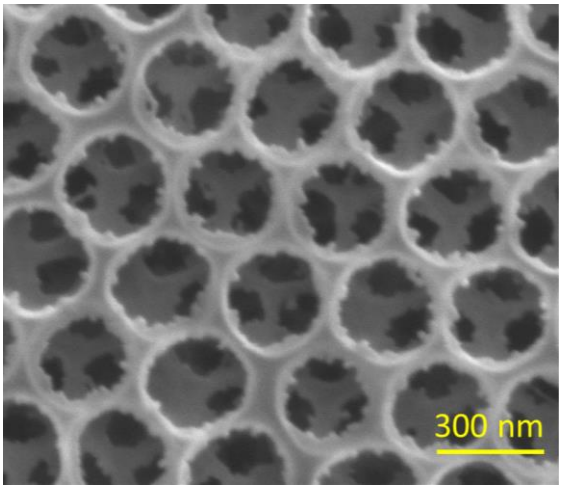

Figure D.1. Top-view SEM image of a PCF showing occupation of 24 particles in an area of 2.187×10^{-6} mm^2.

The concentration of PMMA particles was labeled on the bottle as 4.99×10^{11} particles/mL. Therefore, to obtain one complete monolayer of particles in each trench, 1.1 µL of the suspension in the original PMMA bottle was needed. Since 100 µL of PMMA-TEOS water mixture is used in each trench to make PCF, the ratio of PMMA to PMMA-TEOS-water mixture should be 0.011 in order to form a complete layer. Therefore, for any PMMA-TEOS-water mixture, by dividing the ratio (PMMA / (PMMA-TEOS-water mixture)

by 0.011, the number of layers can be estimated. For example, if the amounts of PMMA, TEOS and water used to fabricate a PCF are 50 μL, 4 μL and 703 μL, respectively, the ratio of PMMA/(PMMA-TEOS-water mixture), which is 50/753, is 0.066. By dividing 0.066 by 0.011, the calculated number of layers resulting from the use of this PMMA-TEOS-water mixture is six.

Appendix E.

Packing density calculation

The packing density for a PCF with a FCC structure can be derived from the following equation[71]:

$$Packing\ density = \frac{N \times \frac{4\pi R^3}{3}}{\alpha^3} \qquad (E.1)$$

Where N, R and α are the number of pores in a single unit cell (the simplest repeating unit in a crystal), radius of the pore and unit cell parameter (physical dimension of unit cell), respectively. Based on Fig. E.1, $\frac{\alpha}{R} = 3.29 \pm 0.15$. Substituting $\frac{\alpha}{R}$ in (E.1), the packing density of the fabricated PCF is 53% ± 6% which means 53% ± 6% of the structure is matrix and 47% ± 6% of the structure is void.

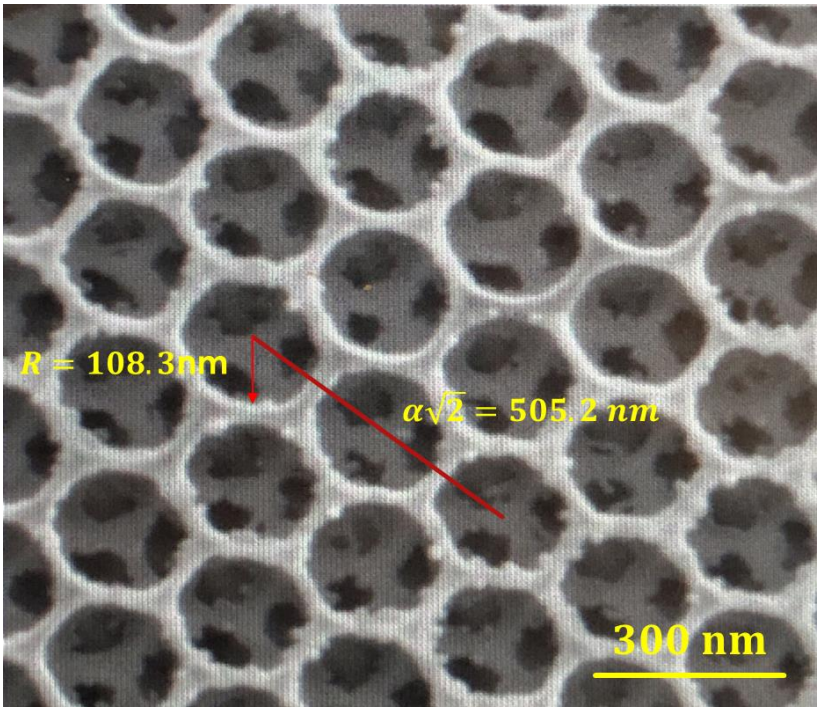

Figure E.1. Top-view SEM image of the fabricated PCF including α (unit cell parameter) and R (radius of the pore).